Article

Releasing a sugar brake generates sweeter tomato without yield penalty

https://doi.org/10.1038/s41586-024-08186-2

Received: 21 January 2024

Accepted: 9 October 2024

Published online: 13 November 2024

Open access

Check for updates

Jinzhe Zhang[1,12], Hongjun Lyu[2,3,12], Jie Chen[2,12], Xue Cao[4], Ran Du[2], Liang Ma[5], Nan Wang[2], Zhiguo Zhu[6], Jianglei Rao[2], Jie Wang[2], Kui Zhong[7], Yaqing Lyu[2], Yanling Wang[2], Tao Lin[8], Yao Zhou[9], Yongfeng Zhou[2], Guangtao Zhu[6], Zhangjun Fei[10], Harry Klee[2] & Sanwen Huang[2,11] ✉

In tomato, sugar content is highly correlated with consumer preferences, with most consumers preferring sweeter fruit[1–4]. However, the sugar content of commercial varieties is generally low, as it is inversely correlated with fruit size, and growers prioritize yield over flavour quality[5–7]. Here we identified two genes, tomato (*Solanum lycopersicum*) *calcium-dependent protein kinase 27* (Sl*CDPK27*; also known as Sl*CPK27*) and its paralogue Sl*CDPK26*, that control fruit sugar content. They act as sugar brakes by phosphorylating a sucrose synthase, which promotes degradation of the sucrose synthase. Gene-edited Sl*CDPK27* and Sl*CDPK26* knockouts increased glucose and fructose contents by up to 30%, enhancing perceived sweetness without fruit weight or yield penalty. Although there are fewer, lighter seeds in the mutants, they exhibit normal germination. Together, these findings provide insight into the regulatory mechanisms controlling fruit sugar accumulation in tomato and offer opportunities to increase sugar content in large-fruited cultivars without sacrificing size and yield.

Tomato is the most valuable vegetable crop, worldwide, and makes substantial overall health and nutritional contributions to the human diet. One key component of tomato fruit quality is the soluble solids content (SSC). Sugars, mainly fructose and glucose, constitute approximately 55% to 65% of the total SSC fraction and 50% of the total solids in the tomato fruit[8]. Sugar content and sugar/acid ratio are the major constituents affecting taste and account for approximately half of overall consumer liking[1]. Most consumers prefer a sweeter tomato[2–4]. Higher sugar content also positively contributes to the economic value for processing tomatoes; an increase of SSC from 4% to 5% could reduce raw material consumption by up to 25% when producing tomato sauce at a sugar concentration of 28% (ref. 9).

Crop domestication is a dynamic and continuous process that strongly reflects human preference. An obvious feature of tomato domestication is the massive increase in fruit size, with cultivated tomatoes being 10–100 times larger than their wild ancestor[10]. However, these increased yields have resulted in a lower sugar content[5,6]. The strong negative correlation between fruit weight and sugar content is probably associated with the loss of high-sugar alleles during domestication and improvement, as photoassimilates must be partitioned into the larger fruits[7,11,12]. As yield and fruit size are the major determinants of variety selection by the industry, breaking this negative correlation between sugar content and yield would be a major breakthrough, especially for consumers.

Genetic, molecular and biochemical characterization of wild tomato species, with high fruit SSC, has greatly improved our understanding of carbohydrate metabolism in tomato, and could potentially be exploited in breeding programmes[13–16]. For example, an acid invertase gene (*TIVI*) from *Solanum chmielewskii* can confer enhanced fruit sugar composition[17,18]. Similarly, a single amino acid change in the product of the *Solanum pennellii* allele for *lycopersicum invertase 5* (*LIN5*) results in a kinetically superior enzyme, thereby increasing the net transport of photoassimilate into the fruit[13]. Introgression of the *FGR*^{H} allele from a wild *Solanum habrochaites* accession (LA1777) into cultivated tomato significantly increased the fructose-to-glucose ratio of ripe fruits[19,20]. Transgenic alterations, by repression or overexpression of various genes, have provided valuable information on the roles of various enzymes in sugar metabolism[4,21–23]. However, an understanding of the genetic and molecular basis of natural variation of tomato fruit sugars remains limited.

The genome-wide association study (GWAS) approach is a powerful technology to dissect complex agronomic traits and identify loci suitable for genetic improvement[24]. The development of metabolomics tools, such as gas chromatography with mass spectrometry (MS) and liquid chromatography with MS/MS, has facilitated comprehensive phenotyping of complex metabolomic traits[11]. Recently, metabolome GWAS has detected many significantly associated loci for tomato sugar accumulation[7,11,25–28]. However, reducing a quantitative trait locus to a

[1]State Key Laboratory of Vegetable Biobreeding, Institute of Vegetables and Flowers, Chinese Academy of Agricultural Sciences, Beijing, China. [2]National Key Laboratory of Tropical Crop Breeding, Shenzhen Branch, Guangdong Laboratory of Lingnan Modern Agriculture, Genome Analysis Laboratory of the Ministry of Agriculture and Rural Affairs, Agricultural Genomics Institute at Shenzhen, Chinese Academy of Agricultural Sciences, Shenzhen, China. [3]Shandong Key Laboratory of Bulk Open-Field Vegetable Breeding, Ministry of Agriculture and Rural Affairs Key Laboratory of Huang Huai Protected Horticulture Engineering, Institute of Vegetables, Shandong Academy of Agricultural Sciences, Jinan, China. [4]State Key Laboratory for Quality Ensurance and Sustainable Use of Dao-di Herbs, Institute of Chinese Materia Medica, China Academy of Chinese Medical Sciences, Beijing, China. [5]State Key Laboratory of Plant Environmental Resilience (SKLPER), College of Biological Sciences, China Agricultural University, Beijing, China. [6]School of Life Sciences, Yunnan Key Laboratory of Potato Biology, Yunnan Normal University, Southwest United Graduate School, Kunming, China. [7]Agriculture and Food Standardization Institute, China National Institute of Standardization, Beijing, China. [8]College of Horticulture, China Agricultural University, Beijing, China. [9]Key Laboratory of Plant Molecular Physiology, Institute of Botany, Chinese Academy of Sciences, China University of Chinese Academy of Sciences, Beijing, China. [10]Boyce Thompson Institute, Cornell University, Ithaca, NY, USA. [11]National Key Laboratory of Tropical Crop Breeding, Chinese Academy of Tropical Agricultural Sciences, Haikou, China. [12]These authors contributed equally: Jinzhe Zhang, Hongjun Lyu, Jie Chen. ✉e-mail: huangsanwen@caas.cn

causative gene can be difficult, and only a few candidate genes have been functionally validated.

Our recent work analysing 33 chemicals specifically associated with consumer preference and flavour intensity yielded a total of 251 associated loci for 20 traits[7]. Two loci were significantly associated with both glucose and fructose contents, corresponding to two major quantitative trait loci, *LIN5* and *SSC11.1* (ref. 7). Here we identified a 12-base-pair (bp) insertion in the promoter of Sl*CDPK27* that is associated with the high-sugar allele of the *SSC11.1* locus. Moreover, genome editing of Sl*CDPK27* and its paralogue Sl*CDPK26* increased glucose and fructose contents by up to 30% without fruit weight or yield penalty, offering an opportunity to engineer sweeter tomatoes in large-fruited cultivars without sacrificing size or yield.

Identification of Sl*CDPK27*

To identify new alleles of genes contributing to sugar accumulation, we performed a GWAS analysis and identified a major peak on chromosome 11, in which the top single nucleotide polymorphism (SNP; ch11_51186147; SL2.50) was strongly associated with SSC ($P = 8.96 \times 10^{-10}$; Fig. 1a), consistent with our previous results[7]. Linkage disequilibrium analysis of the peak region showed that the top SNP is located within an approximately 80-kilobase (kb) block (Fig. 1b) spanning 6 genes. Using a relatively strict *P* value threshold ($P < 1 \times 10^{-6}$), we identified six SNPs in this block that are significantly associated with SSC (Supplementary Table 1), but found that none of these SNPs caused a nonsynonymous mutation. We then examined the expression of the six candidate genes among all accessions. Only *Solyc11g065660*, annotated as encoding *Sl*CDPK27 (ref. 29), exhibited an obvious negatively correlated expression pattern with SSC accumulation (Fig. 1c), indicating that it might act to negatively regulate sugar accumulation.

To fully resolve the DNA sequence variation in Sl*CDPK27*, variants in the genomic sequences of Sl*CDPK27*, including the 2.3-kb promoter region, were identified within 20 accessions. Among these variants, we identified a 12-bp insertion within the promoter region containing several conserved DNA motifs with the core sequence of CAACA (Supplementary Table 2), which could be potentially recognized by RAV transcriptional repressors[30,31]. In addition, we also detected one SNP and one 3-bp deletion in the coding sequence that cause nonsynonymous mutations (Supplementary Table 2). By genotyping these three variants from all accessions, we established that they all showed a significant association with SSC (Extended Data Fig. 1a–c and Supplementary Table 3).

On the basis of these 3 significant variants in Sl*CDPK27*, 344 accessions were classified into 3 haplotype groups (Hap1–Hap3; Fig. 1d). Statistically, the accessions with Hap2 or Hap3, both containing the 12-bp insertion, showed significantly higher SSC than those with Hap1 (Fig. 1d). There was no significant difference in SSC between accessions with Hap2 and those with Hap3, which differ only in the coding sequence, indicating that the 12-bp insertion in the promoter region could be the causal variant. The frequencies of the 12-bp insertion in PIM (local wild relative *Solanum pimpinellifolium* accessions whose fruits weigh about 2 g), CER (*Solanum lycopersicum* var. *cerasiforme* accessions whose fruits weigh about 13 g) and BIG (*S. lycopersicum* accessions whose fruits average about 111 g)[10] indicate that the allele associated with high SSC is prevalent in wild populations, but has largely been lost in modern cultivars (Fig. 1e and Supplementary Table 4).

*Sl*CDPK27 negatively regulates sugar content

To validate the function of Sl*CDPK27* in regulating sugar accumulation, we knocked out Sl*CDPK27* in *S. lycopersicum* Money Maker (MM) and the processing variety M82, using CRISPR–Cas9. Three null mutants for Sl*CDPK27*, named MM-CDPK27-CR1, MM-CDPK27-CR2 and M82-CDPK27-CR3 were obtained (Fig. 2a). MM-CDPK27-CR1 with a 6-bp deletion (from 183 to 188 bp downstream of the start codon) in the ATP-binding domain (Extended Data Fig. 2) is expected to disrupt its kinase activity[32]. MM-CDPK27-CR2 and M82-CDPK27-CR3, with 5-bp deletions (from 184 to 188 bp downstream of ATG), result in the premature termination of protein translation (Extended Data Fig. 2).

To determine whether *Sl*CDPK27 possesses the kinase activity, and whether the L62 and G63 residues absent in the MM-CDPK27-CR1 mutant would disrupt its kinase activity, we purified His-tagged *Sl*CDPK27 and *Sl*CDPK27-CR1 proteins. In vitro kinase assays, using ^{32}P-labelled adenosine triphosphate (ATP), showed that *Sl*CDPK27 is a bona fide kinase (Fig. 2b). Consistent with L62 and G63 being essential for kinase activity, the recombinant *Sl*CDPK27-CR1 mutant protein underwent little to no autophosphorylation (Fig. 2b).

We then selected homozygous MM-CDPK27-CR1, MM-CDPK27-CR2 and M82-CDPK27-CR3 mutant lines without Cas9 for further study. Compared with the wild-type lines, the total SSC and glucose and fructose contents were increased in all three mutants (Fig. 2d–f,h–j). Notably, in the MM-CDPK27-CR1 mutant plants, the total SSC and glucose and fructose contents were increased by 16%, 35% and 30%, respectively. Unexpectedly, no significant differences in fruit weight were detected between wild-type and mutant plants (Fig. 2c,g). These results indicate that *Sl*CDPK27 acts as a negative regulator of sugar accumulation in tomato fruits, and dysfunction of Sl*CDPK27* could significantly increase tomato sugar content without affecting single fruit weight.

Expression pattern of Sl*CDPK27*

To investigate the temporal expression pattern of Sl*CDPK27*, we measured its relative expression, in pericarp tissue, at different stages of fruit development. Analysis using quantitative PCR with reverse transcription (qRT–PCR) revealed that the number of Sl*CDPK27* transcripts increases gradually during fruit ripening, at which stage the fruit size is already fixed (Fig. 3a). This expression pattern is consistent with the role of Sl*CDPK27* as a 'sink gene', regulating the ability of the fruit to store photosynthetic sugars, without affecting the fruit weight.

To further clarify the Sl*CDPK27* expression pattern during fruit development, we generated transgenic plants expressing the *β-glucuronidase* (*GUS*) reporter gene driven by a 2,452-bp promoter of Sl*CDPK27*. The promoter activity of Sl*CDPK27* was measured at different fruit developmental stages, including the immature green, mature green, orange and ripe stages. GUS staining showed that Sl*CDPK27* is expressed at a low level around the vascular tissues of the fruit pericarp at the immature green stages, and its level of expression increases substantially during ripening (Fig. 3b), consistent with the results of qRT–PCR analysis. We observed that Sl*CDPK27* is also expressed in seeds (Fig. 3b), indicating that Sl*CDPK27* may also have a role in seed development.

To determine the subcellular localization of *Sl*CDPK27, we generated *35S*-Sl*CDPK27–GFP* and *35S*-Sl*CDPK27-CR1–GFP* constructs, in which Sl*CDPK27-CR1* contains the mutated Sl*CDPK27* present in the MM-CDPK27-CR1 mutant. When we transiently expressed these two reporters in tobacco leaves, the green fluorescent protein (GFP) fusion protein analysis demonstrated that both *Sl*CDPK27 and *Sl*CDPK27-CR1 were localized at the cell periphery (Fig. 3c), and the two-amino-acid deletion in the MM-CDPK27-CR1 mutant did not affect its subcellular localization.

*Sl*CDPK26 functions redundantly to *Sl*CDPK27

We observed that MM-CDPK27-CR1 showed a greater increase in sugar accumulation than MM-CDPK27-CR2, which is thought to be a typical null mutant for Sl*CDPK27*. Therefore, we reasoned that the higher sugar content in MM-CDPK27-CR1 was caused by the kinase-dead protein functioning in a dominant-negative manner, in which the altered protein product is able to interfere with other kinases. *Sl*CDPK27 belongs to a large calcium-dependent protein kinase (CDPK) family, and there

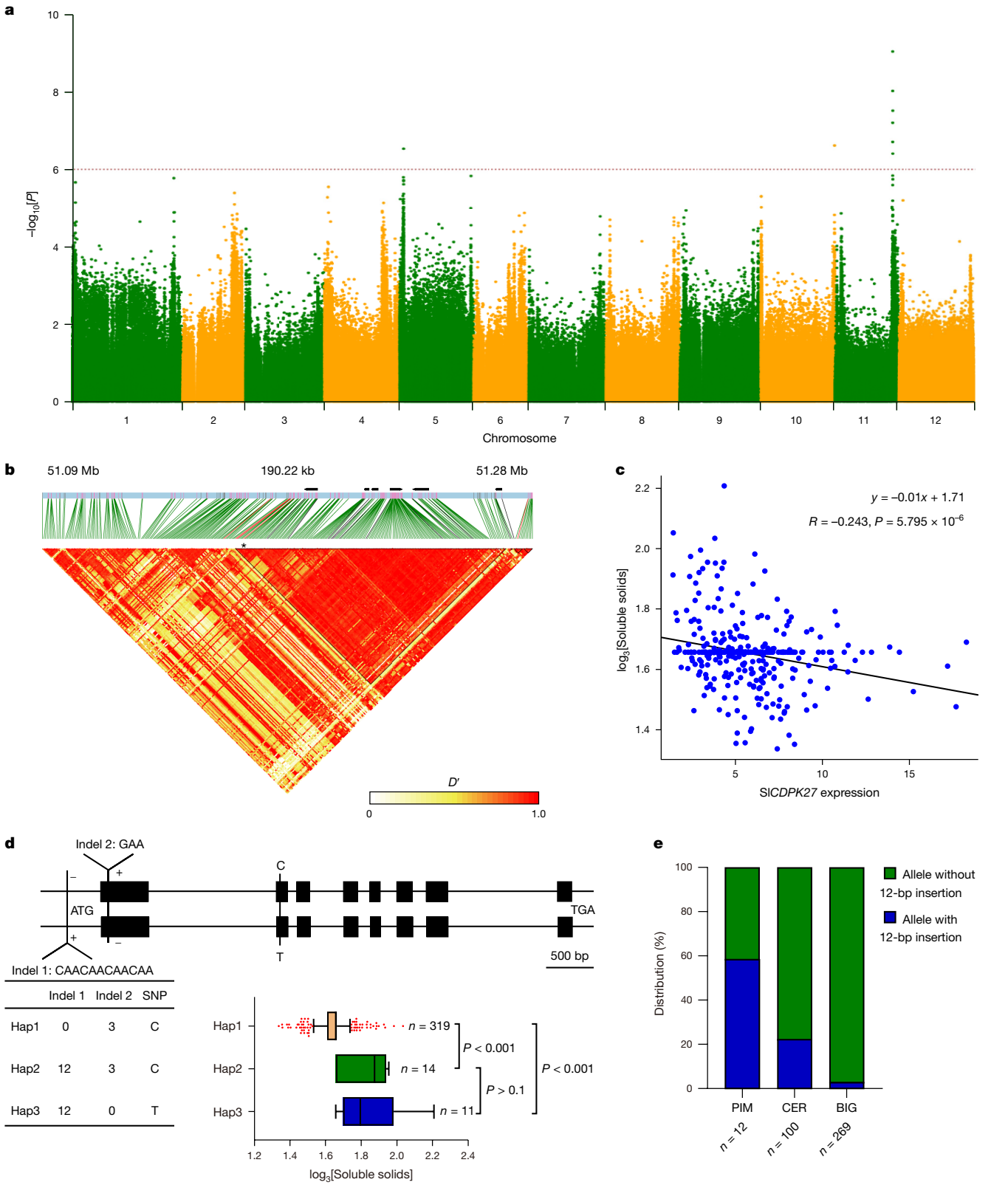

Fig. 1 | Identification and characterization of Sl*CDPK27*. **a**, Manhattan plot of SNPs associated with total SSC. The *y* axis shows the −log scale of *P* values, which was determined using a mixed linear model with a binomial test, implemented in EMMAX. The dotted line denotes the threshold for statistical significance: 1.0×10^{-6} for GWAS. **b**, Linkage disequilibrium plot for SNPs in the 190-kb interval surrounding the leading SNP. Black bars, genes. Asterisk, position of the leading SNP. The colour key (white to red) represents linkage disequilibrium values (*D′*). **c**, Correlation between Sl*CDPK27* expression levels and total SSCs in tomato. The Pearson correlation coefficient (*R*) and its corresponding *P* value, which was calculated from a two-sided test, are indicated at the top. **d**, Haplotypes of Sl*CDPK27* among tomato natural variations. In the box plots, the boxes represent the interquartile range, the line in the middle of each box represents the median, the whiskers represent the interquartile range and the dots represent outlier points; *n* indicates the number of accessions belonging to each haplotype. *P* values were derived by one-way analysis of variance. **e**, Allele distribution of the 12-bp insertion in PIM, CER and BIG groups. *n* indicates the number of accessions in each group.

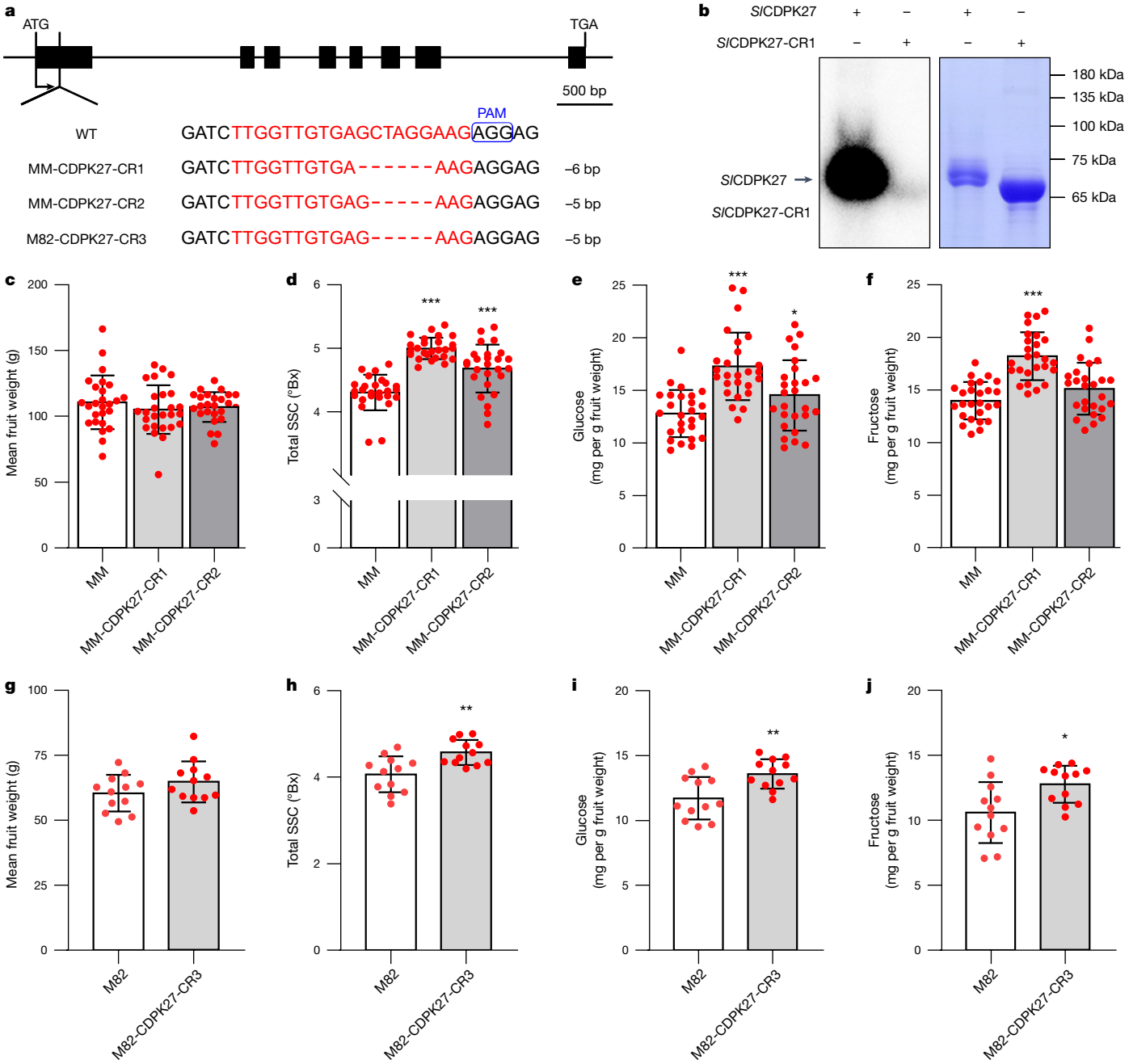

Fig. 2 | Sl*CDPK27* regulates tomato fruit sugar content. a, Generation of mutations in Sl*CDPK27* by CRISPR–Cas9, using a single-guide RNA. Sequences of Sl*CDPK27* in wild-type (WT) and MM-CDPK27-CR1, MM-CDPK27-CR2 and M82-CDPK27-CR3 mutant plants are shown. The sequences targeted by the single-guide RNA are indicated in red, and the protospacer adjacent motif (PAM) sequence is outlined in blue. The deletion is indicated by a dashed line. **b**, In vitro kinase assays verified *Sl*CDPK27 is a bona fide kinase, and the L62 and G63 residues absent in *Sl*CDPK27-CR1 would disrupt its kinase activity. Left, autoradiograph; right, Coomassie brilliant blue staining. **c**, Fruit weight of MM-CDPK27-CR1 and MM-CDPK27-CR2 was not significantly different from that of wild-type plants. **d**–**f**, Both MM-CDPK27-CR1 and MM-CDPK27-CR2 exhibited increased total SSC (**d**) and glucose (**e**) and fructose (**f**) contents, compared to wild-type plants. Values are means ± s.d. ($n = 26$ independent replicates). **g**, Fruit weight of M82-CDPK27-CR3 was not significantly different from that of wild-type plants. **h**–**j**, M82-CDPK27-CR3 exhibited increased total SSC (**h**) and glucose (**i**) and fructose (**j**) contents. Values are means ± s.d. ($n = 12$ independent replicates). In **c**–**j**, a two-tailed Student's *t*-test was used to determine *P* values. $^*P < 0.05$, $^{**}P < 0.01$, $^{***}P < 0.001$, compared to wild-type (MM or M82) plants.

are 29 CDPK proteins in tomato, which could be divided into four groups[29]. *Sl*CDPK27 belongs to group III, with *Sl*CDPK26 (also known as Solyc01g008440) showing the closest evolutionary relationship to *Sl*CDPK27 (Fig. 4a), which led us to test whether *Sl*CDPK26 may function similarly to *Sl*CDPK27.

We first examined the relative expression level of Sl*CDPK26* during fruit development and determined that it is also expressed at increasing levels during fruit ripening, in fruit pericarp tissue (Fig. 4b), temporally overlapping Sl*CDPK27*. Then we mutated Sl*CDPK26* (Extended Data Fig. 3a,b), and found that plants with loss of Sl*CDPK26* function exhibited comparable fruit weight and sugar content to those of the wild-type plants (Extended Data Fig. 3c–f). We also generated an MM-CDPK27-CR2/MM-CDPK26-CR1 double mutant and planted the double mutant as well as the MM-CDPK27-CR1 and MM-CDPK27-CR2

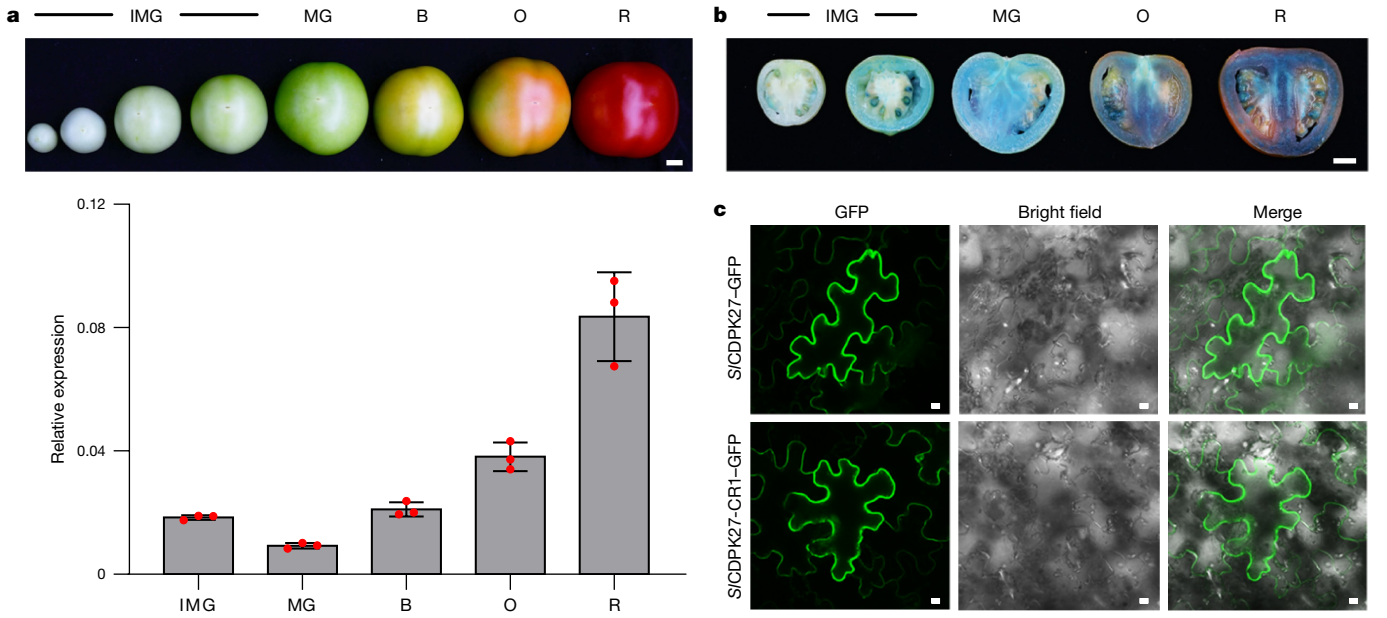

Fig. 3 | The expression pattern and subcellular localization of Sl*CDPK27*. **a**, Relative expression of Sl*CDPK27* at different fruit developmental stages (shown at the top), as calculated relative to the internal reference (Sl*ACTIN*). R, ripe; O, orange; B, breaker; MG, mature green; IMG, immature green. Scale bar, 1 cm. Values are means ± s.d. ($n = 3$ independent replicates). **b**, Analysis of Sl*CDPK27* expression pattern based on GUS staining. Sl*CDPK27* was expressed at the highest level in the ripe fruits. Scale bar, 1 cm. **c**, Subcellular localization of transiently expressed *Sl*CDPK2–GFP and *Sl*CDPK27-CR1–GFP fusion protein in *N. benthamiana* leaves. Scale bars, 10 µm. The subcellular localization assay was repeated three times with similar results.

single mutants (Cas9-free) in two locations (Beijing and Shouguang), and evaluated the sugar content and fruit weight of these mutants in the spring of 2020 and autumn of 2021 (Shouguang), spring of 2022 (Beijing) and spring of 2023 (Beijing). Compared with the wild-type line, all mutant fruits exhibited no obvious differences during fruit development (Fig. 4c), including the final fruit weight (Fig. 4d and Extended Data Fig. 4a,b). Notably, the total SSC and glucose and fructose contents were increased in the mutants, especially in the MM-CDPK27-CR2/MM-CDPK26-CR1 double mutant (Fig. 4e and Extended Data Fig. 4c–g), indicating that simultaneous mutagenesis of Sl*CDPK26* enhances the effects of Sl*CDPK27* on sugar content. We also measured the total fruit yield and fruit number for each plant, collected from six subsequent individual inflorescences. All of the Sl*CDPK*-knockout mutants exhibited comparable fruit yield and fruit number to those of the wild-type line (Fig. 4f,g and Extended Data Fig. 4h,i).

To investigate whether the increased sugar content in these Sl*CDPK*-knockout mutants would improve perceived fruit sweetness, we organized two large-scale sensory evaluation panels, one in March 2022, in Shenzhen, and the other in July 2022, in Beijing. Fruits from the mutants and wild-type lines, which were planted in each of three plots, were tasted by approximately 100 volunteers, who were asked to choose which sample was sweeter. In these sensory panels, fruits from MM-CDPK27-CR1 and the MM-CDPK27-CR2/MM-CDPK26-CR1 double mutant were identified as being significantly sweeter than the wild-type line (Table 1), an outcome consistent with the measured fruit sugar content in each mutant (Fig. 4h,i).

*Sl*CDPK27 and *Sl*CDPK26 phosphorylate *Sl*SUS3

Sucrose synthase (SUS) is a key enzyme that directly hydrolyses sucrose to supply substrates for plant metabolism, and is considered to be a biomarker for plant sink strength[33]. So far, six tomato Sl*SUS* genes have been described. These genes are expressed differentially in different tomato tissues, with the highest level of expression of Sl*SUS3* observed in mature fruits[34]. To elucidate the molecular mechanism modulated by *Sl*CDPK27 in regulating sugar accumulation, we performed immunoprecipitation coupled with MS, using an *Sl*CDPK27 antibody, to screen for potential phosphorylated substrates of *Sl*CDPK27, and identified *Sl*SUS3 as a putative *Sl*CDPK27-interacting protein (Supplementary Table 5).

To further confirm the interaction between *Sl*CDPK27 and *Sl*SUS3, we cloned the Sl*SUS3* full-length coding region, and verified their interaction by yeast two-hybrid assay (Fig. 5a). We also investigated the interaction between *Sl*SUS3 and *Sl*CDPK27 through firefly luciferase (LUC) complementation imaging assays. Fluorescence was observed in the leaf areas co-transformed with the carboxy terminus of LUC fused to *Sl*SUS3 and the amino terminus of LUC fused to *Sl*CDPK27, whereas no detectable fluorescent signal was present in leaf tissue co-transformed with the control plasmids (Fig. 5b). Furthermore, we confirmed the in vivo interaction between *Sl*CDPK26 and *Sl*SUS3 by the LUC complementation imaging assay (Fig. 5c).

As both *Sl*CDPK27 and *Sl*CDPK26 possessed kinase activities and could interact with *Sl*SUS3, we reasoned that *Sl*CDPK27 and *Sl*CDPK26 might directly phosphorylate *Sl*SUS3. In vitro protein kinase assays, using recombinant proteins, supported this hypothesis. His–*Sl*CDPK27 and His–*Sl*CDPK26 directly phosphorylated His–TF–*Sl*SUS3, whereas the mutant protein His–*Sl*CDPK27-CR1 did not (Fig. 5d,e). An examination of the phosphorylation sites in *Sl*SUS3, using liquid chromatography with MS/MS, revealed that S11 was probably phosphorylated by *Sl*CDPK27. We next substituted this serine to alanine (*Sl*SUS3(S11A)), and the resulting *Sl*SUS3(S11A) was no longer phosphorylated by *Sl*CDPK27 and *Sl*CDPK26 (Fig. 5d,e), further supporting that *Sl*CDPK27 and *Sl*CDPK26 mainly phosphorylate *Sl*SUS3 at the S11 residue.

Previous work has indicated that CDPK-mediated phosphorylation of SUS proteins can target SUS for degradation[35]. To investigate the effects of *Sl*SUS3 phosphorylation by *Sl*CDPK27 and *Sl*CDPK26, we performed a cell-free degradation assay. The degradation rate of *Sl*SUS3 was much higher in the wild-type than in MM-CDPK27-CR1 and MM-CDPK27-CR2/MM-CDPK26-CR1 double-mutant extracts (Fig. 5f and Extended Data Fig. 5a), and slightly higher in the wild-type than

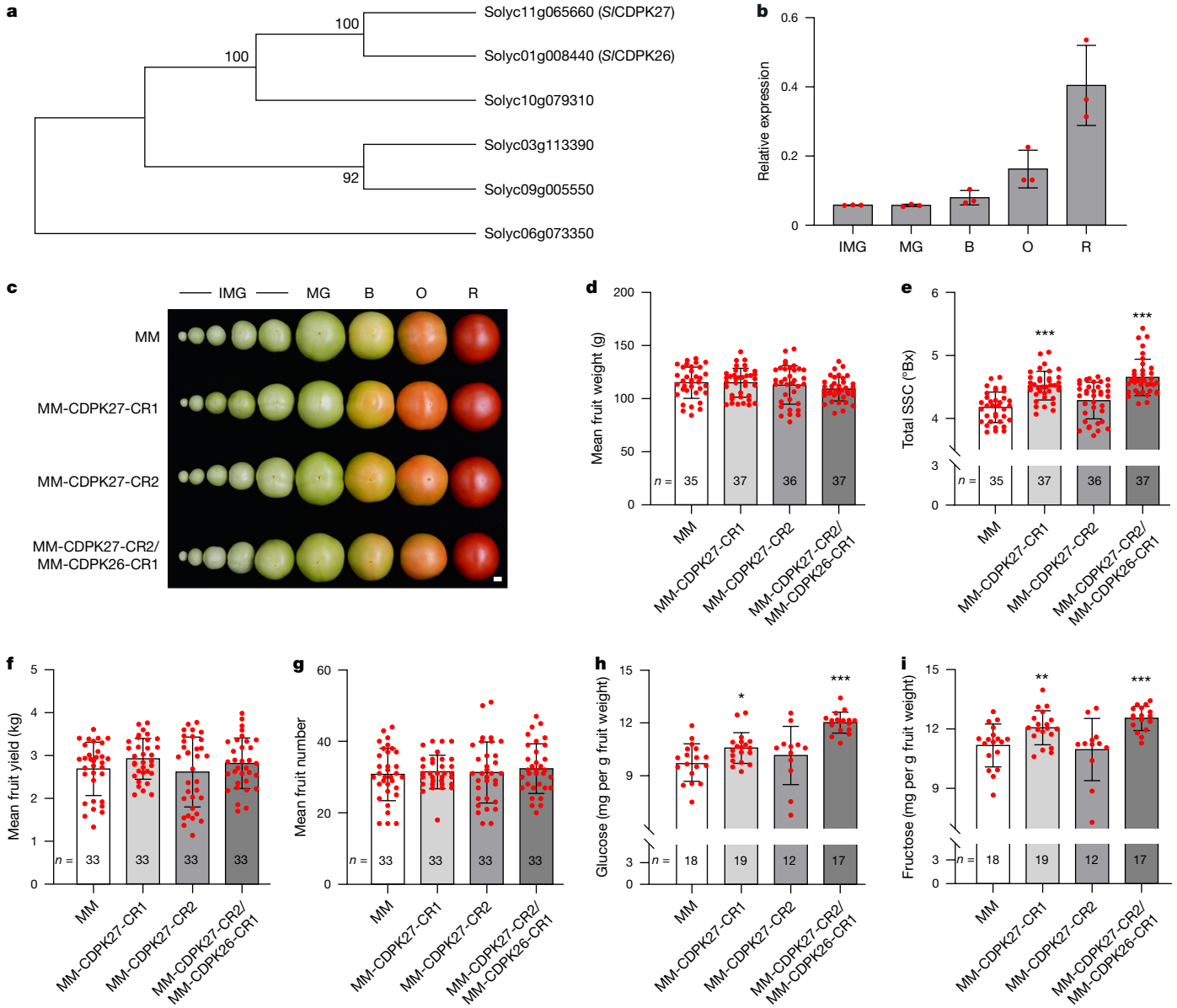

Fig. 4 | *Sl*CDPK26 is functionally redundant to *Sl*CDPK27. a, Phylogenetic analysis of *Sl*CDPK class III family members, based on the maximum-likelihood method. **b**, Relative Sl*CDPK26* expression at different fruit developmental stages, as calculated relative to the internal reference (Sl*ACTIN*). Values are means ± s.d. ($n = 3$ independent replicates). **c**, Fruits of wild-type, MM-CDPK27-CR1, MM-CDPK27-CR2 and MM-CDPK27-CR2/MM-CDPK26-CR1 double-mutant plants at different fruit developmental stages. Scale bar, 1 cm. **d**–**g**, Comparison of fruit weight (**d**), total SSC (**e**), fruit yield (**f**) and fruit number (**g**) between wild-type, MM-CDPK27-CR1, MM-CDPK27-CR2 and MM-CDPK27-CR2/MM-CDPK26-CR1 double-mutant plants, grown in a greenhouse in Beijing in the spring of 2022. **h**,**i**, Comparison of glucose (**h**) and fructose (**i**) contents between wild-type and Sl*CDPK*-knockout mutant plants, which were used for the sensory evaluation panel organized in July 2022, in Beijing. Values are means ± s.d.; *n* represents numbers of biologically independent samples. In **d**–**i**, a two-tailed Student's *t*-test was used to determine *P* values. $^{*}P < 0.05$, $^{**}P < 0.01$, $^{***}P < 0.001$, compared to the wild-type (MM) plants.

in the MM-CDPK27-CR2 or MM-CDPK26-CR1 single-mutant extracts (Extended Data Fig. 5b,c), consistent with the sugar content in each mutant. Moreover, *Sl*SUS3(S11A) showed a much higher stability than *Sl*SUS3 (Fig. 5g). These results further support the hypothesis that *Sl*CDPK27 and *Sl*CDPK26 serve as brakes on fruit sugar metabolism, operating by phosphorylating *Sl*SUS3 at S11, which in turn is degraded.

As *Sl*CDPK27 functions through phosphorylating *Sl*SUS3 to be degraded, we reasoned that overexpression of Sl*SUS3* may also improve the sugar content. We constructed two Sl*SUS3*-overexpressing lines in MM, which are driven by the fruit-specific *E8* promoter[36]. Overexpression of Sl*SUS3* indeed increased the sugar content with little effect on fruit weight (Fig. 5h–l), compared with these features in wild-type plants, similar to the cases of MM-CDPK27-CR1 and the MM-CDPK27-CR2/MM-CDPK26-CR1 double mutant.

*Sl*CDPK27-CR1 inhibits *Sl*SUS3 phosphorylation

The MM-CDPK27-CR1 mutant harbours a kinase-dead version of *Sl*CDPK27 and accumulates more sugar than MM-CDPK27-CR2, which contains only 72 amino acids of the N terminus of *Sl*CDPK27 (named *Sl*CDPK27-CR2). To examine whether *Sl*CDPK27-CR1 could interfere with the function of *Sl*CDPK26, we first analysed the interaction between *Sl*SUS3 and *Sl*CDPK27-CR1, or *Sl*CDPK27-CR2, using LUC complementation imaging assays. The results demonstrated that *Sl*CDPK27-CR1

Table 1 | Sensory evaluation of sweetness for Sl*CDPK*-knockout mutants (March 2022, Shenzhen; July 2022, Beijing)

Mutant	Total number of assessors	Number of correct responses[a]	Minimum number of correct responses required[b]
			α=0.05
MM-CDPK27-CR1 no. 1	105	64*	62
MM-CDPK27-CR1 no. 2	103	76*	61
MM-CDPK27-CR1 no. 3	109	61	64
Mean (Shenzhen)	**106**	**67***	**62**
MM-CDPK27-CR1 no. 1	100	67*	59
MM-CDPK27-CR1 no. 2	100	58	59
MM-CDPK27-CR1 no. 3	100	62*	59
Mean (Beijing)	**100**	**62***	**59**
MM-CDPK27-CR2 no. 1	102	44	60
MM-CDPK27-CR2 no. 2	101	58	60
MM-CDPK27-CR2 no. 3	99	48	59
Mean (Shenzhen)	**101**	**50**	**60**
MM-CDPK27-CR2 no. 1	100	46	59
MM-CDPK27-CR2 no. 2	100	43	59
MM-CDPK27-CR2 no. 3	100	54	59
Mean (Beijing)	**100**	**48**	**59**
MM-CDPK27-CR2/ MM-CDPK26-CR1 no. 1	107	50	63
MM-CDPK27-CR2/ MM-CDPK26-CR1 no. 2	107	72*	63
MM-CDPK27-CR2/ MM-CDPK26-CR1 no. 3	106	63*	62
Mean (Shenzhen)	**107**	**62**	**63**
MM-CDPK27-CR2/ MM-CDPK26-CR1 no. 1	100	73*	59
MM-CDPK27-CR2/ MM-CDPK26-CR1 no. 2	100	58	59
MM-CDPK27-CR2/ MM-CDPK26-CR1 no. 3	100	53	59
Mean (Beijing)	**100**	**61***	**59**

Paired comparison test was used to compare the sweetness of each pair of samples, composed of one Sl*CDPK*-knockout mutant sample and one wild-type MM sample.
The asterisks indicate a significant difference between the number of correct responses and the minimum number of correct responses required at α=0.05.
[a]Value represents the number of assessors who scored the Sl*CDPK*-knockout mutant as sweeter.
[b]Value corresponds to the minimum number of correct responses required for significance, at the level of α=0.05, based on a one-sided paired test (ISO 5495:2005).

could interact with *Sl*SUS3 in *Nicotiana benthamiana* leaves, whereas *Sl*CDPK27-CR2 could not (Fig. 6a). Next we co-expressed Sl*CDPK26*–*nLUC* and *cLUC*–Sl*SUS3* with *35S*-Sl*CDPK27-CR1* or *35S*-Sl*CDPK27-CR2* in two halves of the same *N. benthamiana* leaves, and determined that the fluorescent signals in the halves co-transformed with *35S*-Sl*CDPK27-CR1* were demonstrably weaker than those with *35S*-Sl*CDPK27-CR2* (Fig. 6b), consistent with our hypothesis that *Sl*CDPK27-CR1 can disrupt the interaction between *Sl*SUS3 and *Sl*CDPK26.

As *Sl*CDPK27-CR1 by itself could not phosphorylate *Sl*SUS3, and *Sl*SUS3 was phosphorylated by *Sl*CDPK26 at a high level (Fig. 5d,e), we next performed an in vitro phosphorylation assay to assess whether *Sl*CDPK27-CR1 could affect the phosphorylation capacity of *Sl*CDPK26 against *Sl*SUS3. These assays established that as the amount of *Sl*CDPK27-CR1 was increased, both the phosphorylation level of *Sl*SUS3 by *Sl*CDPK26 and the self-phosphorylation level of *Sl*CDPK26 became weaker, whereas the negative control GST protein had barely no effect (Fig. 6c), indicating that *Sl*CDPK27-CR1 can not only compete with the interaction between *Sl*CDPK26 and *Sl*SUS3, but also affect the *Sl*CDPK26 kinase activity, to protect *Sl*SUS3 from being phosphorylated by *Sl*CDPK26.

Sl*CDPK*-knockout mutants contain fewer, lighter seeds

As noted earlier, Sl*CDPK27* is expressed in seeds, especially at the early stage of seed development (Fig. 3b). On the basis of this finding, we measured the seed number per fruit, and the 1,000-seed weight for each of the mutants. We determined that the seed number of the MM-CDPK27-CR1 mutant fruit was significantly decreased by 18% (Extended Data Fig. 6a), and the 1,000-seed weight of the MM-CDPK27-CR2/MM-CDPK26-CR1 double mutant was 13% lower than that of the wild type (Extended Data Fig. 6b), indicating that deficiency in Sl*CDPKs* had a small negative effect on seed development. However, the MM-CDPK27-CR2/MM-CDPK26-CR1 double mutant exhibited only a slight, but statistically insignificant, decrease in the seed germination rate (Extended Data Fig. 6c). Thus, the minor reduction in seed weight is not expected to affect the suitability of the mutant in commerce.

Compared with the wild-type plants, the Sl*CDPK*-knockout mutants showed a comparable net photosynthetic rate and carbon partitioning rate (Extended Data Fig. 6d,e), indicating that *Sl*CDPK27 and *Sl*CDPK26 do not influence photosynthesis in leaves. Rather, they function as sugar brakes during fruit ripening, probably to modulate the assignment of photoassimilates between fruits and seeds, ensuring adequate energy for seed development.

Co-evolution of *SSC11.1* and fruit weight loci

During tomato domestication and improvement, sugars, which are highly correlated with consumer preferences in fresh tomatoes[1] as well as economic value for processing tomatoes, have been reduced as a potential undesired linkage with increasing fruit weight[7] (Extended Data Fig. 7a). There are multiple fruit weight loci located at the end of chromosome 11, including *fw11.1*, *fw11.2* and *fw11.3*, among which only the gene underlying *fw11.3* has been identified[10,37]. We analysed the causative variation of *fw11.3* in 402 accessions and identified the allele associated with larger fruit, which is prevalent in the BIG population (Supplementary Tables 6 and 7). Sl*CDPK27* is 4.3 Mb from *fw11.3*, and haplotype analysis showed a notable Low-Big haplotype (91.5%) for the *SSC11.1* and *fw11.3* loci within the BIG population (Extended Data Fig. 7b). The local phylogeny suggested an extremely low genetic diversity in both of the loci after domestication (Extended Data Fig. 7c), which may be due to co-evolution of *SSC11.1* and *fw11.3*. A high genetic differentiation (F_{ST}) between the wild and cultivated populations and a reduced Tajima's *D* within the cultivated population were observed, supporting the presence of a large selective sweep region encompassing *SSC11.1* and the three *fw* loci on chromosome 11 (50.5–56.3 Mb). An extremely low recombination rate in this region suggests limited dissociation of these candidate sites[11] (Extended Data Fig. 7d,e). Furthermore, analysis of runs of homozygosity demonstrated a positive correlation between homozygous genomic region lengths and inbreeding levels, consistent with the low recombination rate. Notably, a significantly higher level of inbreeding was detected in the BIG population, with some varieties reaching genome-wide homozygosity (Extended Data Fig. 7f). Collectively, these results indicate a high level of genomic linkage generated by inbreeding, contributing to the frequency-dependent selection of the low-SSC phenotype, probably owing to the selection of larger fruit.

Conservation of *Sl*CDPK27 and *Sl*CDPK26

To investigate the conservation of *Sl*CDPK27 and *Sl*CDPK26 outside tomato, we curated a dataset of 12 plant genomes encompassing angiosperms, gymnosperms and ferns, and identified 337 protein sequences

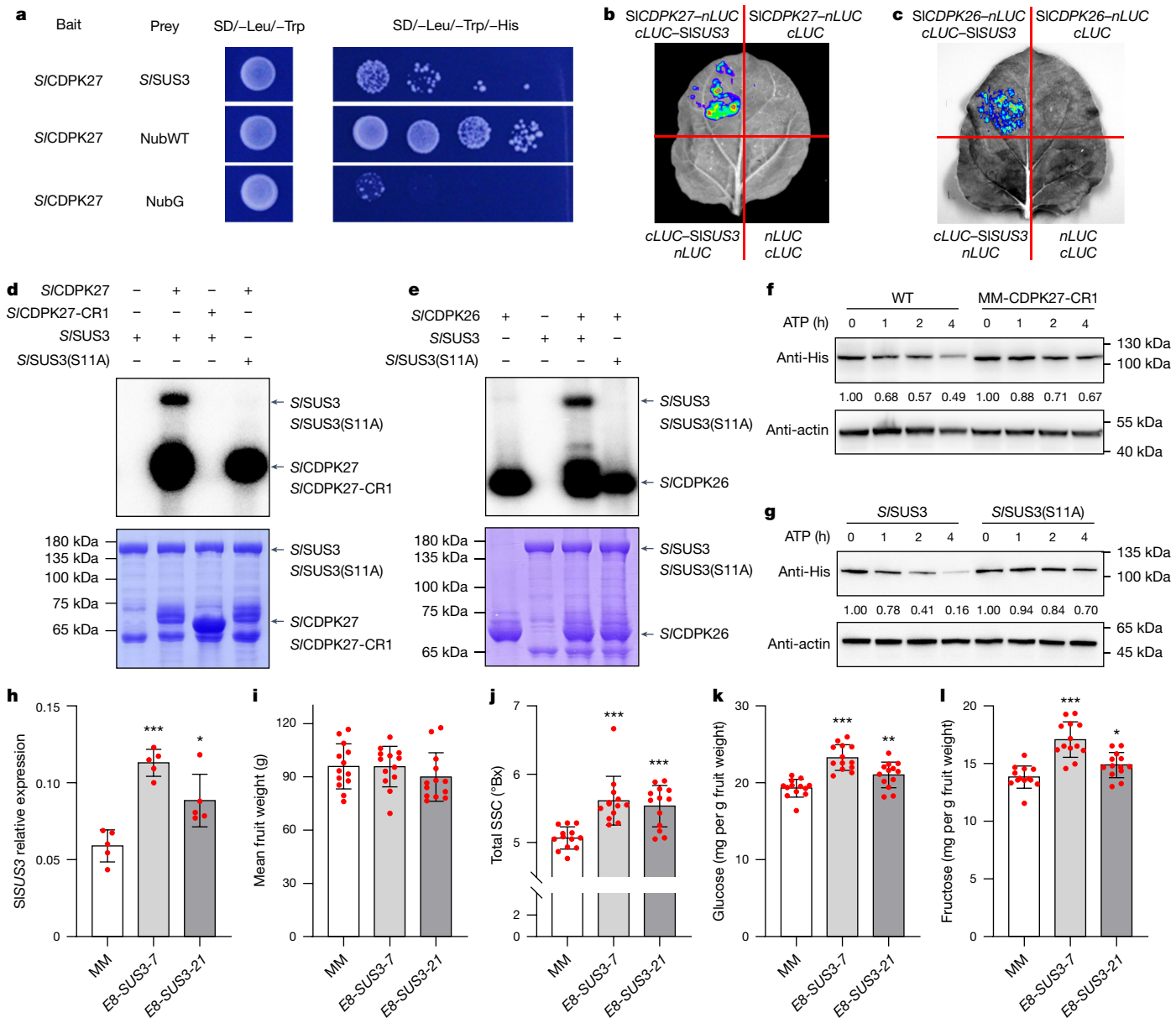

Fig. 5 | *Sl*CDPK27 and *Sl*CDPK26 interact with and phosphorylate *Sl*SUS3. **a**, Yeast two-hybrid assay indicates that *Sl*CDPK27 and *Sl*SUS3 interact in yeast. The N-terminal half of ubiquitin (NubWT) was used as the positive control; the N-terminal half of ubiquitin with I13 substituted to glycine (NubG) was used as the negative control. Transformed yeasts were spotted on the control medium SD/−Leu/−Trp (medium lacking leucine and tryptophan) or the selective medium SD/−Leu/−Trp/−His (medium lacking leucine, tryptophan and histidine). **b**,**c**, Split firefly LUC complementation imaging assay, performed in mature *N. benthamiana* leaves, shows that *Sl*CDPK27 (**b**) and *Sl*CDPK26 (**c**) interact with *Sl*SUS3 in planta. **d**,**e**, *Sl*CDPK27 (**d**) and *Sl*CDPK26 (**e**) phosphorylate *Sl*SUS3 at the S11 residue, in vitro. Top, autoradiograph; bottom, Coomassie brilliant blue staining. **f**, Mutation of Sl*CDPK27* attenuates *Sl*SUS3 degradation in a cell-free assay. **g**, *Sl*SUS3(S11A) degraded at a slower rate than *Sl*SUS3 in a cell-free assay. **h**, Relative expression of Sl*SUS3*. Values are means ± s.d. ($n = 5$ independent replicates). **i**–**l**, Comparison of fruit weight (**i**), total SSC (**j**) and glucose (**k**) and fructose (**l**) contents between wild-type and Sl*SUS3*-overexpressing plants. Values are means ± s.d. ($n = 13$ independent replicates). In **h**–**l**, a two-tailed Student's *t*-test was used to determine *P* values. $^{*}P < 0.05$, $^{**}P < 0.01$, $^{***}P < 0.001$, compared to the wild-type (MM) plants.

belonging to the CDPK family. Phylogenetic analysis revealed that these CDPKs could be divided into four distinct clades, with both *Sl*CDPK26 and *Sl*CDPK27 belonging to clade III (Extended Data Fig. 8a), consistent with previous reports[29,38]. Given the relatively close relationship between *Sl*CDPK26 and *Sl*CDPK27 within clade III, we focused our investigation on this specific clade. Sequence alignments indicated a high degree of conservation between *Sl*CDPK26, *Sl*CDPK27 and their orthologues, and the two deleted amino acids in MM-CDPK27-CR1, leucine and glycine, are conserved in almost all of the *Sl*CDPK27 and *Sl*CDPK26 orthologues (Extended Data Fig. 8b). Moreover, sequence conservation was also observed in the gymnosperm *Ginkgo biloba* (Extended Data Fig. 8b), indicating potential functional similarities across diverse plant lineages.

Discussion

Sugars are powerful regulators of organ growth and development, and are intertwined with fruit weight in a complex and dynamic relationship[7,39]. Tomato fruit weight relies on cell division and cell enlargement, events that occur in the green developing fruit. Fruit quality, including sugar content, is largely determined during the ripening process[40]. However, previous studies have largely focused on manipulation of

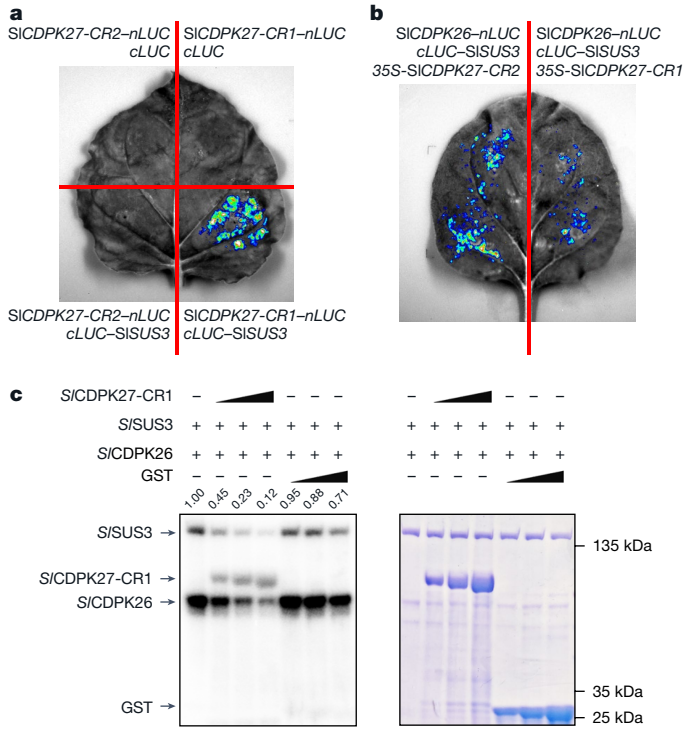

Fig. 6 | *Sl*CDPK27-CR1 suppresses the *Sl*CDPK26-mediated *Sl*SUS3 phosphorylation. a, Split firefly LUC complementation assay shows that *Sl*CDPK27-CR1, but not *Sl*CDPK27-CR2, interacts with *Sl*SUS3 in mature *N. benthamiana* leaves. **b**, *Sl*CDPK27-CR1 interferes with the interaction between *Sl*CDPK26 and *Sl*SUS3, in vivo. Fluorescent signals were much weaker in leaf halves co-transformed with cLUC–*Sl*SUS3, *Sl*CDPK26–nLUC and 35S-*Sl*CDPK27-CR1, compared with cLUC–*Sl*SUS3, *Sl*CDPK26–nLUC and 35S-*Sl*CDPK27-CR2. **c**, *Sl*CDPK27-CR1 inhibits the phosphorylation of *Sl*SUS3 by *Sl*CDPK26. Relative protein abundance of phosphorylated *Sl*SUS3 is indicated at the top of the gel. Left, autoradiograph; right, Coomassie brilliant blue staining. The in vitro kinase competition experiment was repeated four times with similar results.

sugar metabolic enzymes that are expressed throughout fruit development, resulting in improved sugar content at the expense of reduced fruit weight[40,41]. One of the main goals of modern tomato breeding is to increase fruit sugar concentration while increasing or at least maintaining fruit size, which has largely proved elusive[6,7]. However, some recent studies advocate that this goal should be possible, such as through the genetic approach of recurrent selection[42], simultaneously manipulating certain biophysical factors and transmembrane transports[43], and taking a phenotype-guided approach, using a large enough population[44]. Here we identified a high-sugar allele that has been selectively lost during domestication and improvement, probably because of its co-evolution with fruit weight loci. Sl*CDPK27* and its paralogue Sl*CDPK26* are expressed at increasing levels during fruit ripening, at which stage they act as brakes on sugar content in fruit tissues through phosphorylation and subsequent degradation of *Sl*SUS3. By genome editing of Sl*CDPK27* and Sl*CDPK26*, we increased SSC in the large-fruited cultivars, thereby establishing sweeter tomatoes, as assessed by consumer panels, without fruit weight or yield penalty. These findings provide insight into the genetic and molecular regulatory mechanisms controlling fruit sugar accumulation in tomato and offer opportunities to further increase sugar content in large-fruited cultivars without sacrificing size and yield.

Success of flowering plants depends greatly on producing vigorous seeds and effective seed dispersal[45]. Tomato fruit ripening is a highly coordinated developmental process that provides both a suitable environment for seed maturation and a mechanism for their dispersal[46]. Ripening tomato fruits, with their soft flesh and ready supply of sugars and other nutrients, attract small rodents and birds[47]. In plants, multiple sinks compete for the available photoassimilates, generating a priority system among them[48]. Tomato, in its natural environment, is a perennial plant. The *Sl*CDPKs work as sugar brakes during fruit ripening, probably as a mechanism to ensure adequate sugar or energy for seed development. However, seeds within a tomato fleshy-fruited variety are primed, in situ, during the later developmental stages, and seed dry weight reaches a plateau after the fruit has reached the mature green stage[49,50]. In this study, we showed that a deficiency in Sl*CDPKs* increases fruit sugar content and decreases seed number, or weight, but with normal germination, indicating that photoassimilates can be reallocated from seeds, into fruits, during ripening. However, the interaction between seeds and fruits remains poorly understood in tomato, and whether *Sl*CDPKs directly regulate seed development, or indirectly affect seed development by regulating energy distribution, will require further investigation. Future studies could evaluate the assignment of photoassimilates between fruits and seeds, which may provide an opportunity to store more energy in fruits, without affecting seed quality.

Genetic variation is the driving force for crop improvement and natural variations in wild species have been widely used for tomato improvement[41]. However, naturally occurring mutations are relatively limited, and increasing attention has been given to developing new allelic variations for some well-studied genes[51–53]. In our study, *Sl*CDPK27-CR1 mutants accumulated more sugar than *Sl*CDPK27-CR2, owing to a dominant-negative interaction. This phenomenon is reminiscent of the spontaneous *nor* and *rin* mutants, which also function as dominant-negative mutations instead of loss-of-function mutations[54–56]. Functional redundancy is common in the plant kingdom, serving as a resource for generation of new variants, potentially providing more beneficial alleles for crop improvement, but also potentially interfering with processes as dominant-negative interactors.

The γ-aminobutyric acid-enriched tomato, developed using CRISPR–Cas9 technology, is commercially available in Japan, opening the way for genome-edited fruits, especially for global tomato markets[57,58]. Sugar content is the primary determinant of fruit taste, and agricultural yield of processing tomatoes is determined by the fruit weight and the total SSC, predominantly consisting of sugars. Higher sugar content will not only positively influence consumer fruit likeability, but also reduce costs associated with processing tomatoes[40]. Our finding of the sugar brake genes, Sl*CDPK27* and Sl*CDPK26*, and especially the creation of the Sl*CDPK27-CR1* allele, provides a possible solution for improving sugar content without reduction in fruit yield for modern commercial varieties, which are preferred by both consumers and producers, and CRISPR-edited 'sweetness-promoting' tomatoes may be available to consumers in the near future.

Online content

Any methods, additional references, Nature Portfolio reporting summaries, source data, extended data, supplementary information, acknowledgements, peer review information; details of author contributions and competing interests; and statements of data and code availability are available at https://doi.org/10.1038/s41586-024-08186-2.

1. Colantonio, V. et al. Metabolomic selection for enhanced fruit flavor. *Proc. Natl Acad. Sci. USA* **119**, e2115865119 (2022).
2. Gough, C. & Hobson, G. E. A comparison of the productivity, quality, shelf-life characteristics and consumer reaction to the crop from cherry tomato plants grown at different levels of salinity. *J. Hortic. Sci.* **65**, 431–439 (1990).
3. Kader, A. A. Flavor quality of fruits and vegetables. *J. Sci. Food Agric.* **88**, 1863–1868 (2008).
4. Beckles, D. M. Factors affecting the postharvest soluble solids and sugar content of tomato (*Solanum lycopersicum* L.) fruit. *Postharvest Biol. Technol.* **63**, 129–140 (2012).
5. Cong, B., Barrero, L. S. & Tanksley, S. D. Regulatory change in YABBY-like transcription factor led to evolution of extreme fruit size during tomato domestication. *Nat. Genet.* **40**, 800–804 (2008).

6. Prudent, M. et al. Genetic and physiological analysis of tomato fruit weight and composition: influence of carbon availability on QTL detection. *J. Exp. Bot.* **60**, 923–937 (2009).
7. Tieman, D. et al. A chemical genetic roadmap to improved tomato flavor. *Science* **355**, 391–394 (2017).
8. Davies, J. N. & Hobson, G. E. The constituents of tomato fruit — the influence of environment, nutrition, and genotype. *Crit. Rev. Food Sci. Nutr.* **15**, 205–280 (1981).
9. Wang, B. et al. Enhanced soluble sugar content in tomato fruit using CRISPR/Cas9-mediated *SlINVINH1* and *SlVPE5* gene editing. *PeerJ* **9**, e12478 (2021).
10. Lin, T. et al. Genomic analyses provide insights into the history of tomato breeding. *Nat. Genet.* **46**, 1220–1226 (2014).
11. Zhu, G. et al. Rewiring of the fruit metabolome in tomato breeding. *Cell* **172**, 249–261 (2018).
12. Bertin, N. et al. Seasonal evolution of the quality of fresh glasshouse tomatoes under Mediterranean conditions, as affected by air vapour pressure deficit and plant fruit load. *Ann. Bot.* **85**, 741–750 (2000).
13. Fridman, E., Carrari, F., Liu, Y.-S., Fernie, A. R. & Zamir, D. Zooming in on a quantitative trait for tomato yield using interspecific introgressions. *Science* **305**, 1786–1789 (2004).
14. Chetelat, R. T., Deverna, J. W. & Bennett, A. B. Effects of the *Lycopersicon chmielewskii sucrose accumulator gene* (*sucr)* on fruit yield and quality parameters following introgression into tomato. *Theor. Appl. Genet.* **91**, 334–339 (1995).
15. Husain, S. E., Thomas, B. J., Kingston-Smith, A. H. & Foyer, C. H. Invertase protein, but not activity, is present throughout development of *Lycopersicon esculentum* and *L. pimpinellifolium* fruit. *New Phytol.* **150**, 73–81 (2001).
16. Stommel, J. R. Enzymic components of sucrose accumulation in the wild tomato species *Lycopersicon peruvianum*. *Plant Physiol.* **99**, 324–328 (1992).
17. Klann, E. M., Chetelat, R. T. & Bennett, A. B. Expression of *acid invertase* gene controls sugar composition in tomato (*Lycopersicon*) fruit. *Plant Physiol.* **103**, 863–870 (1993).
18. Klann, E. M., Hall, B. & Bennett, A. B. Antisense *acid invertase* (*TIV1*) gene alters soluble sugar composition and size in transgenic tomato fruit. *Plant Physiol.* **112**, 1321–1330 (1996).
19. Levin, I., Gilboa, N., Yeselson, E., Shen, S. & Schaffer, A. A. *Fgr*, a major locus that modulates the fructose to glucose ratio in mature tomato fruits. *Theor. Appl. Genet.* **100**, 256–262 (2000).
20. Shammai, A. et al. Natural genetic variation for expression of a SWEET transporter among wild species of *Solanum lycopersicum* (tomato) determines the hexose composition of ripening tomato fruit. *Plant J.* **96**, 343–357 (2018).
21. Patrick, J. W., Botha, F. C. & Birch, R. G. Metabolic engineering of sugars and simple sugar derivatives in plants. *Plant Biotechnol. J.* **11**, 142–156 (2013).
22. Petreikov, M. et al. Carbohydrate balance and accumulation during development of near-isogenic tomato lines differing in the *AGPase-L1* allele. *J. Am. Soc. Hort. Sci.* **134**, 134–140 (2009).
23. Powell, A. L. T. et al. *Uniform ripening* encodes a Golden 2-like transcription factor regulating tomato fruit chloroplast development. *Science* **336**, 1711–1715 (2012).
24. Nordborg, M. & Weigel, D. Next-generation genetics in plants. *Nature* **456**, 720–723 (2008).
25. Zhou, Y. et al. Graph pangenome captures missing heritability and empowers tomato breeding. *Nature* **606**, 527–534 (2022).
26. Zhao, J. et al. Meta-analysis of genome-wide association studies provides insights into genetic control of tomato flavor. *Nat. Commun.* **10**, 1534 (2019).
27. Sauvage, C. et al. Genome-wide association in tomato reveals 44 candidate loci for fruit metabolic traits. *Plant Physiol.* **165**, 1120–1132 (2014).
28. Zhao, J. et al. Association mapping of main tomato fruit sugars and organic acids. *Front. Plant Sci.* **7**, 1286 (2016).
29. Wang, J.-P., Xu, Y.-P., Munyampundu, J.-P., Liu, T.-Y. & Cai, X.-Z. *Calcium-dependent protein kinase* (*CDPK*) and *CDPK-related kinase* (*CRK*) gene families in tomato: genome-wide identification and functional analyses in disease resistance. *Mol. Genet. Genomics* **291**, 661–676 (2016).
30. Castillejo, C. & Pelaz, S. The balance between CONSTANS and TEMPRANILLO activities determines *FT* expression to trigger flowering. *Curr. Biol.* **18**, 1338–1343 (2008).
31. Kagaya, Y., Ohmiya, K. & Hattori, T. RAV1, a novel DNA-binding protein, binds to bipartite recognition sequence through two distinct DNA-binding domains uniquely found in higher plants. *Nucleic Acids Res.* **27**, 470–478 (1999).
32. Lu, S. et al. CDD/SPARCLE: the conserved domain database in 2020. *Nucleic Acids Res.* **48**, D265–D268 (2020).
33. Stein, O. & Granot, D. An overview of sucrose synthases in plants. *Front. Plant Sci.* **10**, 95 (2019).
34. Dinh, Q.-D. et al. Exploring natural genetic variation in tomato sucrose synthases on the basis of increased kinetic properties. *PLoS ONE* **13**, e0206636 (2018).
35. Hardin, S. C. et al. Phosphorylation of sucrose synthase at serine 170: occurrence and possible role as a signal for proteolysis. *Plant J.* **35**, 588–603 (2003).
36. Deikman, J. et al. Separation of *cis* elements responsive to ethylene, fruit development, and ripening in the 5′-flanking region of the ripening-related *E8* gene. *Plant Mol. Biol.* **37**, 1001–1011 (1998).
37. Mu, Q. et al. Fruit weight is controlled by cell size regulator encoding a novel protein that is expressed in maturing tomato fruits. *PLoS Genet.* **13**, e1006930 (2017).
38. Hu, Z. et al. Genome-wide identification and expression analysis of calcium-dependent protein kinase in tomato. *Front. Plant Sci.* **7**, 469 (2016).
39. Yamaki, S. Metabolism and accumulation of sugars translocated to fruit and their regulation. *J. Jpn. Soc. Hortic. Sci.* **79**, 1–15 (2010).
40. Beckles, D. M., Hong, N., Stamova, L. & Luengwilai, K. Biochemical factors contributing to tomato fruit sugar content: a review. *Fruits* **67**, 49–64 (2011).
41. Rothan, C., Diouf, I. & Causse, M. Trait discovery and editing in tomato. *Plant J.* **97**, 73–90 (2019).
42. Yamamoto, E. et al. A simulation-based breeding design that uses whole-genome prediction in tomato. *Sci. Rep.* **6**, 19454 (2016).
43. Chen, J. et al. Modelling predicts tomatoes can be bigger and sweeter if biophysical factors and transmembrane transports are fine-tuned during fruit development. *New Phytol.* **230**, 1489–1502 (2021).
44. Zemach, I. et al. Multi-year field trials provide a massive repository of trait data on a highly diverse population of tomato and uncover novel determinants of tomato productivity. *Plant J.* **116**, 1136–1151 (2023).
45. Lorts, C. M., Briggeman, T. & Sang, T. Evolution of fruit types and seed dispersal: a phylogenetic and ecological snapshot. *J. Syst. Evol.* **46**, 396 (2008).
46. Klee, H. J. & Giovannoni, J. J. Genetics and control of tomato fruit ripening and quality attributes. *Annu. Rev. Genet.* **45**, 41–59 (2011).
47. Tanksley, S. D. The genetic, developmental, and molecular bases of fruit size and shape variation in tomato. *Plant Cell* **16**, S181–S189 (2004).
48. Lemoine, R. et al. Source-to-sink transport of sugar and regulation by environmental factors. *Front. Plant Sci.* **4**, 272 (2013).
49. Valdes, V. M. & Gray, D. The influence of stage of fruit maturation on seed quality in tomato (*Lycopersicon lycopersicum* (L.) Karsten). *Seed Sci. Technol.* **26**, 309–318 (1998).
50. Demir, I. & Samit, Y. Seed quality in relation to fruit maturation and seed dry weight during development in tomato. *Seed Sci. Technol.* **29**, 453–462 (2001).
51. Muños, S. et al. Increase in tomato locule number is controlled by two single-nucleotide polymorphisms located near *WUSCHEL*. *Plant Physiol.* **156**, 2244–2254 (2011).
52. Xu, C. et al. A cascade of arabinosyltransferases controls shoot meristem size in tomato. *Nat. Genet.* **47**, 784–792 (2015).
53. Rodríguez-Leal, D., Lemmon, Z. H., Man, J., Bartlett, M. E. & Lippman, Z. B. Engineering quantitative trait variation for crop improvement by genome editing. *Cell* **171**, 470–480 (2017).
54. Gao, Y. et al. Re-evaluation of the *nor* mutation and the role of the NAC-NOR transcription factor in tomato fruit ripening. *J. Exp. Bot.* **71**, 3560–3574 (2020).
55. Wang, R. et al. Re-evaluation of transcription factor function in tomato fruit development and ripening with CRISPR/Cas9-mutagenesis. *Sci. Rep.* **9**, 1696 (2019).
56. Vrebalov, J. et al. A MADS-box gene necessary for fruit ripening at the tomato *ripening-inhibitor* (*rin*) locus. *Science* **296**, 343–346 (2002).
57. Waltz, E. GABA-enriched tomato is first CRISPR-edited food to enter market. *Nat. Biotechnol.* **40**, 9–11 (2021).
58. Nonaka, S., Arai, C., Takayama, M., Matsukura, C. & Ezura, H. Efficient increase of ɣ-aminobutyric acid (GABA) content in tomato fruits by targeted mutagenesis. *Sci. Rep.* **7**, 7057 (2017).

Methods

Plant materials

The 402 tomato accessions used in this study are listed in Supplementary Table 8. Cultivated tomato lines, MM and M82, were used for the transgenic experiments. All of the tomato materials used in this study were grown in a greenhouse. The experimental plant materials in Figs. 2 and 4 and Extended Data Fig. 4b,e,h,i were grown in a greenhouse at the Beijing experimental station (40° 13′ 58.66″ N, 116° 06′ 47.32″ E, Beijing, China) in the autumn of 2018, and the spring of 2020, 2022 and 2023. The experimental plant materials in Extended Data Fig. 4a,d,f,g and Extended Data Fig. 4c were grown in a greenhouse at the Shouguang experimental station (36° 54′ 21″ N, 118° 51′ 46″ E, Shandong, China) in the autumn of 2021 and spring of 2020, respectively. Tomato seedlings were grown in a commercial nursery for 30–40 days and then transplanted to the greenhouse. The tomato plants were provided special care with adequate supply of water and fertilizer, and diseased plants were removed as soon as they were found. If the inflorescence was abnormally developed, a maximum of eight fruits were retained for each inflorescence. For the analyses of fruit yield, we collected all of the fruits from six subsequent individual inflorescences, until they were ripe. The fruit weight was determined per inflorescence. Total yield was the sum of fruit weight from each inflorescence for each plant. Plants that were diseased or grown in guard rows were marked and excluded from the analyses.

For fruit developmental analysis, the harvested fruit was divided into five categories, according to their maturity stage: immature green, mature green, breaker, orange and ripe based on the tomato colour chart USDA Visual Aid TM-L-1 (ref. 59). Only fruits that appeared developmentally equivalent were used for analysis. The pericarp of six fruits was excised, immediately frozen in liquid nitrogen, ground by means of a cryogenic mill and stored at −80 °C for further analysis. *N. benthamiana* used in this study was grown in a growth chamber with a light/dark photoperiod of 8/16 h at 25 °C.

Association mapping

We used the previously reported SNP dataset for the GWAS analysis[7] with the EMMAX program[60]. The matrix of pairwise genetic distances was used as the variance–covariance matrix for random effects, and the first ten principal components were included as fixed effects. The genome-wide significance threshold was set as $P = 1/n$, in which n is the effective number of independent SNPs. The effective number of independent SNPs was calculated using Genetic type 1 Error Calculator software[61]. The significant P value threshold was $P = 1.0 \times 10^{-6}$. The Haploview software was used to calculate linkage disequilibrium, with the following parameters: -maxdistance 2,000 -minMAF 0.05 -hwcutoff 0 (ref. 62). Pairwise linkage disequilibrium between the SNPs in the 200-kb interval surrounding the leading SNP was evaluated.

For association analysis of Sl*CDPK27* PCR amplification data with SSC, a total of 65 variants were generated. An SNP and 3-bp deletion, which lead to nonsynonymous mutation, and a 12-bp insertion, which could be recognized by RAV transcriptional repressor[30,31], were retained for further analysis. Information on the variants is listed in Supplementary Table 2. For allelic variation analysis of Sl*CDPK27*, a dataset of the three key variants was obtained through PCR amplification. The SNP, 12-bp insertion and 3-bp deletion were used to access haplotypes of Sl*CDPK27*; only haplotypes with a total number of accessions of ≥3 were analysed. All primers used in this study are shown in Supplementary Table 9.

Transgenic functional validation

The single-guide RNAs for CRISPR–Cas9 constructs were designed using the CRISPRdirect tool (http://crispr.dbcls.jp/). The CRISPR–Cas9 binary vectors (pKSE402) were revised from the pKSE401 vector by replacing AtU6p with *Sl*U6p (ref. 63). The recombinant pKSE402 vectors were designed to produce mutagenesis within the coding sequence of Sl*CDPK27* and Sl*CDPK26*, using single-guide RNAs in combination with the *Cas9* endonuclease gene (Fig. 2a and Extended Data Fig. 3a for the single-guide RNAs used in this study). Vectors with the correct insertion were introduced into *Agrobacterium tumefaciens* strain AGL1 competent cells, and tomato transformation was performed as described previously[64]. The transgenic lines were confirmed by PCR and sequencing. All experiments were performed using homozygous lines without T-DNA integration.

Physicochemical analysis

More than six red ripe fruits were collected from each line, and each fruit was measured for fruit weight and total SSC. The SSC was determined using a digital refractometer (PAL-1, ATAGO), adjusted and calibrated at 20 °C with distilled water and expressed as degrees Brix.

Content analysis of sugars

More than six red ripe fruits were collected from each line for sugar analysis. The mixed fruit pericarp was ground in liquid nitrogen, and then 200 mg of ground powder was diluted in 1.4 ml of extraction buffer, with internal standard (8 mg arabinose). After sonication for 10 min and centrifugation (13,000 r.p.m.) for 10 min, the supernatants were filtered through a 0.22-μm polyethersulfone ultrafiltration membrane, twice, and then added to a solution of 100 μl extraction buffer, 895 μl acetonitrile and 5 μl 20% ammonia water for analysis. The content was measured by ultra-performance liquid chromatography with MS/MS (ACQUITY UPLC I-Class-Xevo TQ-S Micro, Waters). The detection was performed as described previously[64].

For sugar analysis, an ACQUITY UPLC BEH Amide 1.7-μm column was used (2.1 × 100 mm; Waters). The mobile phase was composed of acetonitrile as solvent A, and 0.1% ammonia water as solvent B. The temperatures of the column and autosampler were 60 °C and 4 °C, respectively. Each sugar was separated by increasing solvent B from 10% to 20% in 2 min, keeping at 20% for 6 min, changing to 25% in 0.1 min, keeping at 25% for 1.9 min, then changing to 20% in 1 min and keeping at 20% for 2 min. The flow rate was 0.2 ml min^{-1}. Data analysis was performed using MassLynx V4.1 (Waters).

RNA isolation and qRT–PCR

Total RNA was extracted from the fruit pericarp harvested at the ripening stages, using the RNA extraction kit (catalogue no. 0416-50, HUAYUEYANG Biotechnology), and the RNA was reverse transcribed, using GoScript Reverse Transcriptase (catalogue no. A5003; Promega), according to the manufacturer's instructions. qPCR was performed using GoScript qPCR Master Mix (catalogue no. A6001; Promega) and the Bio-Rad CFX-96 real-time PCR with CFX Maestro 1.1 software (Bio-Rad). The relative expression levels of each gene were calculated using the $2^{-\Delta Ct}$ method. Three technical replicates were used to calculate the C_T value, and three to five biological replicates were analysed. The tomato *ACTIN* gene (*Solyc03g078400*) was used as the internal reference.

Histochemical GUS staining

To examine the Sl*CDPK27* expression pattern by GUS staining, the 2,452-bp Sl*CDPK27* promoter region upstream of the ATG was amplified from genomic DNA. Then, the products were cloned into pENTR/D-TOPO to generate pENTR-*Sl*CDPK27pro. *Sl*CDPK27pro-GUS was generated by an LR reaction between pKGWFS7 and pENTR-*Sl*CDPK27pro. *Sl*CDPK27pro-GUS vector was then introduced into *A. tumefaciens* strain AGL1 competent cells, and tomato transformation was performed as described previously[64].

Different tomato tissues from the *Sl*CDPK27pro-GUS transgenic lines were collected and incubated in GUS staining buffer containing 5-bromo-4-chloro-3-indolylb-D-glucuronide (X-gluc) as a substrate. Samples were incubated at 37 °C for 1 h. After incubation, the staining buffer was then changed to 70% ethanol for decolourizing.

Subcellular localization assay

To detect the subcellular localization of *Sl*CDPK27 protein, full-length cDNAs of Sl*CDPK27* and Sl*CDPK27-CR1* were amplified from MM and the MM-CDPK27-CR1 mutant. The amplified fragments were cloned into pDONR/Zeo (Invitrogen) to generate pENTR-*Sl*CDPK27 or pENTR-*Sl*CDPK27-CR1, respectively. The *Sl*CDPK27–GFP and *Sl*CDPK27-CR1–GFP constructs were generated by LR reactions between pK7FWG2 and pENTR-*Sl*CDPK27 or pENTR-*Sl*CDPK27-CR1, respectively. Then, *Sl*CDPK27–GFP and *Sl*CDPK27-CR1–GFP were transformed into *A. tumefaciens* strain GV3101, and the agrobacteria harbouring the constructs were infiltrated into *N. benthamiana* leaves. The plants were then grown in the dark for 24 h, followed by 48 h in a greenhouse under normal conditions. The transient GFP fluorescence in *N. benthamiana* leaf cells was observed under a Leica SP8 confocal microscope.

Sensory evaluation of sweetness

The sensory evaluation panel was organized twice (one in Shenzhen in March 2022, and the other in Beijing in July 2022). In this study, approximately 100 participants (aged 20–59 years) were selected for each of the sensory tests. These participants were required to be healthy and without any known oral diseases. The sensory test followed the Declaration of Helsinki, and the experimental protocol was approved by the Ethical Committee of Agricultural Genomics Institute at Shenzhen, Chinese Academy of Agricultural Sciences. All participants were informed about the sources of the genome-edited tomato materials and the sensory procedure beforehand, and signed informed consent forms before the sensory tests.

The two-alternative forced-choice test was performed to compare the difference in the sensory properties of the sweetness between fruits harvested from Sl*CDPK*-knockout mutants and wild-type MM plants. A paired sample, consisting of a wild-type MM (control sample) and a Sl*CDPK*-knockout mutant (test sample) fruit, was evaluated, according to ISO 5495:2005 (ref. 65). A total of three test samples were evaluated in this study, including MM-CDPK27-CR1, MM-CDPK27-CR2 and MM-CDPK27-CR2/MM-CDPK26-CR1 double-mutant plants. Each test sample was evaluated three times, and each time fruit was picked from three different plots. Each sample was placed in a transparent tasting cup labelled with random codes, and the paired samples were presented to the sensory assessors, for sensory evaluation, in a balanced order.

For each panel, about 100 volunteer assessors were asked to perform all of the tests. They were asked to evaluate pairs of samples and were required to indicate the sweeter sample of the paired tomato fruits. A 20–30 s break was provided between the different samples, and the assessors were requested to thoroughly rinse their mouths with purified water. Binomial distribution was used for the statistical analysis of paired comparison tests (ISO 5495:2005)[65]. If the number of correct responses was greater than or equal to the minimum number of correct responses required, at a specified significance level (in this study, $\alpha = 0.05$), it can be concluded that the Sl*CDPK*-knockout mutant sample has a higher sweetness than the wild-type MM sample. Otherwise, the difference was not significant. After the sensory evaluation, every six remaining fruits of each type were mixed into one sample for further glucose and fructose content analysis. Owing to COVID-19, we did not collect fruits for the sensory evaluation panel organized in Shenzhen in March 2022.

*Sl*CDPK27 antibody production

A peptide containing 15 amino acids from the 6th to the 20th amino acids of *Sl*CDPK27 (^{6}GTPGNSSENKKKKNK^{20}) was synthesized and used as an antigen to produce polyclonal antibodies in rabbits. The antibodies were purified by an antigen-specific affinity approach by Shanghai Youke Biotechnology Co., Ltd.

Immunoprecipitation coupled with MS

For identification of the interaction proteins of *Sl*CDPK27 by immunoprecipitation coupled with MS, fruits of MM at the red ripe stage were collected and ground in liquid nitrogen with an IKA A11 basic analytical mill (A11BS025). Total proteins were extracted with extraction buffer (300 mM Tris-HCl pH 8.0, 600 mM NaCl, 4 mM $MgCl_2$, 0.5% Triton X-100, complete EDTA-free protease inhibitor cocktail (Roche, cOmplete) and phosphatase inhibitor cocktail (Roche, PhosSTOP)). The extracts were centrifuged at 12,000 r.p.m. for 20 min, and the supernatants were incubated with anti-*Sl*CDPK27 (1:100 dilution) at 4 °C overnight, with the supernatant incubated with IgG used as the control, and then Pierce protein A/G magnetic beads (Thermo Fisher Scientific, 88802) were used to immunoprecipitate the *Sl*CDPK27 protein. The immunocomplex was washed three times and resuspended with 100 µl extraction buffer. A 10 µl volume of sample was used for western blot analysis with *Sl*CDPK27 antibodies (1:2,000 dilution), and horseradish peroxidase-conjugated goat anti-rabbit IgG (H + L) (ZSGB-BIO, catalogue no. ZB-2301, 1:10,000 dilution) was used as the secondary detection antibody. The remaining magnetic beads were separated on 10% SDS–PAGE gels, and then sent to PTM BIO Co., Ltd (Hangzhou, China) for analysis by liquid chromatography coupled with MS/MS.

Yeast two-hybrid assay

The yeast two-hybrid assays were performed using DUAL membrane starter kits (P01401-P01429, Shanghai OE Biotech) according to the manufacturer's instructions. The ubiquitin moiety was split into two halves, and the N-terminal half with I13 substituted to glycine was used to prevent nonspecific binding to the C-terminal half of ubiquitin. The full-length cDNA of Sl*CDPK27* was cloned into the pBT3-STE bait vector to generate NubG–*Sl*CDPK27 and the full-length cDNA of Sl*SUS3* was cloned into the pPR3-N prey vector to generate Cub–*Sl*SUS3, by gateway cloning. The fusion plasmids were co-transformed into yeast strain NMY51 and the yeast transformants were screened on SD/−Leu/−Trp and SD/−Leu/−Trp/−His selective medium.

Firefly LUC complementation imaging assay

The full-length cDNAs of Sl*CDPK27*, Sl*CDPK27-CR1*, Sl*CDPK27-CR2* and Sl*CDPK26* were cloned into the pCAMBIA-nLUC-GW vector to generate *Sl*CDPK27–nLUC, *Sl*CDPK27-CR1–nLUC, *Sl*CDPK27-CR2–nLUC and *Sl*CDPK26–nLUC, respectively. Then the full-length cDNA of Sl*SUS3* was cloned into the pCAMBIA-cLUC-GW vector to generate cLUC–*Sl*SUS3, by gateway cloning[66]. The plasmids were transformed into *A. tumefaciens* strain GV3101. Different combinations shown in Figs. 5b,c and 6a,b were co-infiltrated into *N. benthamiana* leaves. The plants were placed in the dark for 24 h, followed by 48 h in a growth chamber under long-day conditions (16 h light and 8 h dark). Then, the infiltrated *N. benthamiana* leaves were sprayed with 1 mM luciferin, in 0.01% Triton X-100 solution, and kept in darkness for 5 min to quench the fluorescence. A deep cooling CCD imaging apparatus (LB985 Night SHADE) was used to capture the fluorescence image in Fig. 5b, and the Tanon-5200 image system (Tanon, Shanghai, China) was used to capture the fluorescence images in Figs. 5c and 6a,b.

Recombinant protein production and purification

The full-length cDNAs of Sl*SUS3* were cloned into the pCold-TF vector to express His–TF-tagged recombinant protein. The site-specific mutation in Sl*SUS3*^{SIIA} was introduced by PCR, with the primers listed in Supplementary Table 9. The mutated fragments, confirmed by Sanger sequencing, were cloned into the pCold-TF vector to express His–TF-tagged recombinant protein. The full-length cDNAs of Sl*CDPK27*, Sl*CDPK27-CR1*, Sl*CDPK26*, Sl*SUS3* and Sl*SUS3*^{SIIA} were cloned into the pET28GW vector to express His-tagged recombinant protein, by gateway cloning. The full-length cDNA of Sl*CDPK27-CR1* was also cloned

into the pGEX-4T-1 vector to express GST-tagged recombinant protein for the in vitro kinase competition experiment. His–*Sl*CDPK27, His–*Sl*CDPK27-CR1, GST–*Sl*CDPK27-CR1, His–*Sl*CDPK26, His–*Sl*SUS3, His–SUS3(S11A), His–TF–*Sl*SUS3, His–TF–*Sl*SUS3(S11A) and GST protein were expressed in *Escherichia coli* Rosetta (DE3) (catalogue no. EC1010, Shanghai Weidi Biotechnology), following induction with 1 mM isopropyl *β*-D-1-thiogalactopyranoside (IPTG) at 16 °C for 16 h, and then were purified using Ni-NTA resin (GE-Healthcare) and glutathione Sepharose 4B (GE-Healthcare) according to the manufacturer's instructions.

In vitro phosphorylation assays

For the in vitro kinase assays, purified recombinant kinases (His–*Sl*CDPK27, His–*Sl*CDPK27-CR1 or His–*Sl*CDPK26) and substrate (His–TF–SlSUS3 or His–TF–*Sl*SUS3(S11A)) were incubated at 30 °C in a kinase reaction buffer (50 mM Tris-HCl, pH 7.5, 10 mM $MgCl_2$, 1 mM dithiothreitol (DTT), 10 μCi [γ-^{32}P]ATP) for 30 min. The reactions were then stopped by adding 5× SDS loading buffer (250 mM Tris-HCl, pH 6.8, 10% (w/v) SDS, 0.5% bromophenol blue, 50 mM DTT and 50% glycerol) and boiled for 5 min. The samples were then separated on 10% SDS–PAGE gels. After electrophoresis, the gels were stained with Coomassie brilliant blue as a loading control, and the phosphorylated proteins were visualized by autoradiography.

For the in vitro kinase competition experiment, GST–*Sl*CDPK27-CR1 and GST proteins with various concentration gradients were first incubated with His–TF–*Sl*SUS3 at 30 °C for 1 h. Then, His–*Sl*CDPK26 was added to the kinase reaction buffer for another 30 min. The reactions were stopped by adding 5× SDS loading buffer and boiled for 5 min. The samples were separated on 10% SDS–PAGE gels and visualized by autoradiography.

Identification of phosphorylation sites of *Sl*SUS3 by *Sl*CDPK27

For analysis of phosphorylation sites of *Sl*SUS3 in vitro, recombinant His–*Sl*CDPK27 and His–TF–*Sl*SUS3 proteins were incubated in kinase reaction buffer (50 mM Tris-HCl, pH 7.5, 10 mM $MgCl_2$, 1 mM DTT, 0.25 mM ATP) at 30 °C for 30 min. Next, the proteins were separated on 10% SDS–PAGE gel, and the bands of His–TF–*Sl*SUS3 were cut out. Then, the His–TF–*Sl*SUS3 protein was digested with trypsin and subjected to analysis by liquid chromatography with MS/MS by the biological MS laboratory at the College of Biological Sciences at China Agricultural University.

Cell-free protein degradation assay

The cell-free protein degradation assay for *Sl*SUS3 and *Sl*SUS3(S11A) was performed as described previously[67,68]. Briefly, total proteins were extracted from full-red ripe fruits of wild-type, MM-CDPK27-CR1, MM-CDPK27-CR2, MM-CDPK26-CR1 and MM-CDPK27-CR2/MM-CDPK26-CR1 double mutant plants, in degradation buffer (300 mM Tris-HCl at pH 8.0, 600 mM NaCl, 4 mM $MgCl_2$ and 20 mM DTT). Recombinant His–*Sl*SUS3 and His–SUS3(S11A) protein and 5 mM ATP were added to the extracts. The mixtures were incubated at room temperature (25 °C) for 1, 2 and 4 h. The reactions were stopped by the addition of SDS sample buffer. His–*Sl*SUS3, His–SUS3(S11A) and actin proteins were detected by immunoblotting with anti-His (MBL, catalogue no. D291-3, 1:3,000 dilution) and anti-actin (Sigma, catalogue no. A0480, 1:10,000 dilution) antibodies, and horseradish peroxidase-conjugated goat anti-mouse IgG (H + L) (ZSGB-BIO, catalogue no. ZB-2305, 1:10,000 dilution) was used as the secondary detection antibody. Protein gel blot images were scanned, and the intensity of the images was quantified by ImageJ (National Institutes of Health).

Gas exchange and $^{13}CO_2$ labelling of tomato

In vivo isotopic labelling with $^{13}CO_2$ and flux estimation throughout leaf photosynthetic metabolism were performed as described previously[69]. A 30-l positive-pressure environmental chamber set at 28 °C, 50% humidity and around 200 μmol m^{-2} s^{-1} light intensity was applied for labelling. After displacing CO_2 with premixed gas with a N_2/O_2 ratio of 78/22, 4-week-old plants were labelled using premixed gas containing $^{13}CO_2$ (Cambridge Isotope Laboratories) at a $^{13}CO_2/N_2/O_2$ ratio of 0.33:78:21.967. Then, samples labelled for 0, 5, 10 and 20 min were collected and immediately frozen with liquid nitrogen, and then stored at −80 °C for further analysis.

Analysis of metabolite labelling

A 100 ± 3 mg quantity of ground powder of each sample was used for analysis of labelled metabolites. A 1.2 ml volume of extraction buffer (dichloromethane/methanol 2:1) was added to 100 ± 3 mg ground powder of each sample, and 300 μl water was added after vortexing five times. Then, 600 μl supernatant was transferred to a new tube and dried under nitrogen after centrifugation at 12,000*g* for 10 min. After resuspension with 80 μl water, the samples were incubated in a refrigerator at 4 °C for 10 min, and the supernatants were collected for analysis by liquid chromatography with MS after 10-min centrifugation twice at 12,000*g* to remove the precipitates.

A Dionex Ultimate 3000 UPLC system coupled with a TSQ Quantiva Ultra triple-quadrupole mass spectrometer (Thermo Fisher) equipped with a heated electrospray ionization probe was used for detection. Extracts were separated by a Synergi Hydro-RP column (2.0 × 100 mm, 2.5 μm, Phenomenex). A binary solvent system was used, with mobile phase A consisting of 10 mM tributylamine adjusted with 15 mM acetic acid in water, and mobile phase B consisting of pure methanol, using a 25-min gradient with mobile B gradually increased from 5% to 90%. Data were acquired in selected reaction monitoring mode for metabolites in positive-negative ion switching mode (Supplementary Table 10). The resolutions for Q1 and Q3 are both 0.7 full-width at half-maximum. The source voltage was 3,500 V for positive and 2,500 V for negative ion mode. The source parameters were as follows: capillary temperature, 350°C; heater temperature, 300 °C; sheath gas flow rate, 35; auxiliary gas flow rate, 10. Tracefinder 3.2 (Thermo) was used for metabolite identification and peak integration.

Genetic statistics and estimation of inbreeding

The variation map was constructed using previously published data[7]. Subsequently, the phylogeny was used to examine the population structure on the basis of the genome-wide SNPs using the IQTREE program (version 2.1.4)[70]. The 12-bp insertion and 1,406-bp deletion were combined to investigate the frequency of haplotypes of *SSC11.1* and *fw11.3* among PIM and BIG populations. To clarify the selective pattern of *SSC11.1* (ch11_51.180–51.205 Mb; SL2.50) and *fw11.3* (ch11_55.250–55.290 Mb; SL2.50), the independent phylogenies were constructed with the 'GTR + I + G' model using IQTREE[70].

The genetic statistics were combined to examine the selection in the large region containing *SSC11.1* and three fruit weight (*fw*) loci (ch11_48.0–56.3 Mb; SL2.50). Tajima's *D* test compares the observed distribution of pairwise nucleotide differences to the expected distribution under a neutral model of evolution. A negative value suggests an excess of low-frequency mutations, which could be indicative of directional selection, population contraction or genetic hitchhiking[71]. The pairwise differentiation (F_{ST}), known as the fixation index, is a measure of genetic differentiation between populations. High F_{ST} values typically suggest high divergence between populations[71]. Tajima's *D* value was analysed by VCFtools (version 0.1.16), and the F_{ST} value was calculated using the Python script popgenWindows.py as described previously[72,73]. The recombination rate could be estimated on the basis of demographic history and the variation map, and SMC++ was used to infer the demographic history of BIG and PIM populations[74]. In addition, the variation map of PIM and BIG was integrated in Pyrho to evaluate the genome-wide recombination rate[75].

Runs of homozygosity (ROHs) are extended stretches of homologous segments within genomes that reveal population history and trait architecture[76]. These regions indicate a lack of genetic variation and

are often associated with inbreeding or recent ancestry. We performed the genome-wide ROH analysis on the basis of the variation map using the PLINK program (version 1.90b6.21)[77] with the following parameters: --homozyg-kb 1,000 --homozyg-snp 10 --homozyg-window-het 3. Increased inbreeding levels are associated with both longer and more numerous ROHs. Furthermore, recent inbreeding events tend to result in longer ROH segments. To visualize these patterns, we used ggplot2 (version 3.4.4)[78] to plot ROH length and number distributions across wild (PIM) and cultivated (BIG) populations.

Phylogenetic analysis of *Sl*CDPK27 and *Sl*CDPK26

Conserved domains and their corresponding Pfam-formatted HMM models (PF13499 and PF00069) were identified for *Sl*CDPK26 and *Sl*CDPK27 proteins by leveraging the InterPro database. Subsequently, genome sequence and annotation files encompassing a diverse array of 12 genomes were used for phylogenetic and sequence analyses, including a fern (*Azolla filiculoides*; https://fernbase.org/ftp/), a gymnosperm (*G. biloba*; https://ginkgo.zju.edu.cn/genome/ftp/; version-2021) and 10 angiosperm crops: *S. lycopersicum* (https://solgenomics.sgn.cornell.edu/organism/Solanum_lycopersicum/genome; SL2.50), *Solanum melongena* (https://solgenomics.sgn.cornell.edu/organism/Solanum_melongena/genome; HQ-1315), *Solanum tuberosum* (https://genome.jgi.doe.gov/portal/; DMv6.1), *Arabidopsis thaliana* (https://genome.jgi.doe.gov/portal/; TAIR10), *Capsicum annuum* (http://www.pepperbase.site/node/3; CaT2T), *Malus domestica* (https://genome.jgi.doe.gov/portal/; v1.1), *Manihot esculenta* (https://genome.jgi.doe.gov/portal/; v8.1), *Oryza sativa* (https://genome.jgi.doe.gov/portal/; v7.0), *Citrus sinensis* (http://citrus.hzau.edu.cn/download.php; v3.0) and *Citrullus lanatus* (http://cucurbitgenomics.org/organism/21; 97103, v2). The names of protein annotations are assigned abbreviations derived from their scientific names for consistency. Homologous protein annotation was performed utilizing the hmmer program (version 3.4)[79] and the previously identified Pfam-formatted HMM models. The annotated protein sequences were subjected to multiple sequence alignment using MAFFT (version 7.525)[80] and phylogenetic tree construction using the neighbour-joining method in the MEGA program (version 11.0.10)[81]. Sequence alignment of CDPK proteins in clade III was visualized using the ggmsa (version 3.19)[82] package in R.

Reporting summary

Further information on research design is available in the Nature Portfolio Reporting Summary linked to this article.

Data availability

All data are available in this article and its Supplementary Information (Supplementary Tables 1–10). Original uncropped gel and blot images are provided in Supplementary Figs. 1 and 2. HMM models were downloaded from the InterPro database (https://www.ebi.ac.uk/interpro/entry/pfam). Source data are provided with this paper.

Code availability

No customized code was generated in this study.

59. United States Department of Agriculture. *Color classification requirements in United States standards for grades of fresh tomatoes.* USDA Visual Aid TM-L-1 (USDA, 1975).
60. Kang, H. M. et al. Variance component model to account for sample structure in genome-wide association studies. *Nat. Genet.* **42**, 348–354 (2010).
61. Li, M.-X., Yeung, J. M. Y., Cherny, S. S. & Sham, P. C. Evaluating the effective numbers of independent tests and significant *p*-value thresholds in commercial genotyping arrays and public imputation reference datasets. *Hum. Genet.* **131**, 747–756 (2012).
62. Barrett, J. C., Fry, B., Maller, J. & Daly, M. J. Haploview: analysis and visualization of LD and haplotype maps. *Bioinformatics* **21**, 263–265 (2005).
63. Xing, H.-L. et al. A CRISPR/Cas9 toolkit for multiplex genome editing in plants. *BMC Plant Biol.* **14**, 327 (2014).
64. Li, R. et al. *FIS1* encodes a GA2-oxidase that regulates fruit firmness in tomato. *Nat. Commun.* **11**, 5844 (2020).
65. Stone, H. & Sidel, J. L. *Sensory Evaluation Practices* 3rd edn (Academic Press, 2004).
66. Zhang, J. et al. The *Arabidopsis* RING-type E3 ligase TEAR1 controls leaf development by targeting the TIE1 transcriptional repressor for degradation. *Plant Cell* **29**, 243–259 (2017).
67. Liu, L. et al. An efficient system to detect protein ubiquitination by agroinfiltration in *Nicotiana benthamiana*. *Plant J.* **61**, 893–903 (2010).
68. Ye, K. et al. BRASSINOSTEROID-INSENSITIVE2 negatively regulates the stability of transcription factor ICE1 in response to cold stress in Arabidopsis. *Plant Cell* **31**, 2682–2696 (2019).
69. Ma, F., Jazmin, L. J., Young, J. D. & Allen, D. K. Isotopically nonstationary ^{13}C flux analysis of changes in *Arabidopsis thaliana* leaf metabolism due to high light acclimation. *Proc. Natl Acad. Sci. USA* **111**, 16967–16972 (2014).
70. Chernomor, O., von Haeseler, A. & Minh, B. Q. Terrace aware data structure for phylogenomic inference from supermatrices. *Syst. Biol.* **65**, 997–1008 (2016).
71. Okazaki, A., Yamazaki, S., Inoue, I. & Ott, J. Population genetics: past, present, and future. *Hum. Genet.* **140**, 231–240 (2021).
72. Danecek, P. et al. The variant call format and VCFtools. *Bioinformatics* **27**, 2156–2158 (2011).
73. Martin, S. H., Davey, J. W. & Jiggins, C. D. Evaluating the use of ABBA-BABA statistics to locate introgressed loci. *Mol. Biol. Evol.* **32**, 244–257 (2015).
74. Terhorst, J., Kamm, J. A. & Song, Y. S. Robust and scalable inference of population history from hundreds of unphased whole genomes. *Nat. Genet.* **49**, 303–309 (2017).
75. Spence, J. P. & Song, Y. S. Inference and analysis of population-specific fine-scale recombination maps across 26 diverse human populations. *Sci. Adv.* **5**, eaaw9206 (2019).
76. Ceballos, F. C., Joshi, P. K., Clark, D. W., Ramsay, M. & Wilson, J. F. Runs of homozygosity: windows into population history and trait architecture. *Nat. Rev. Genet.* **19**, 220–234 (2018).
77. Purcell, S. et al. PLINK: a tool set for whole-genome association and population-based linkage analyses. *Am. J. Hum. Genet.* **81**, 559–575 (2007).
78. Wickham, H. ggplot2. *WIREs Comput. Stat.* **3**, 180–185 (2011).
79. Finn, R. D., Clements, J. & Eddy, S. R. HMMER web server: interactive sequence similarity searching. *Nucleic Acids Res.* **39**, W29–W37 (2011).
80. Katoh, K., Misawa, K., Kuma, K. & Miyata, T. MAFFT: a novel method for rapid multiple sequence alignment based on fast Fourier transform. *Nucleic Acids Res.* **30**, 3059–3066 (2002).
81. Kumar, S., Stecher, G., Li, M., Knyaz, C. & Tamura, K. MEGA X: molecular evolutionary genetics analysis across computing platforms. *Mol. Biol. Evol.* **35**, 1547–1549 (2018).
82. Zhou, L. et al. ggmsa: a visual exploration tool for multiple sequence alignment and associated data. *Brief. Bioinform.* **23**, bbac222 (2022).

Acknowledgements We thank W. J. Lucas for input on manuscript preparation; X. Cui, S. Zhang and H. Wang for assistance with transgenic experiments and sugar content analyses; Z. Huang, J. Yan, K. Ye, Y. Wu, Z. Fan, M. Su and J. Ma for experimental assistance; and X. Liu, X. Wang and L. Wang for assistance with $^{13}CO_2$ labelling experiments. This work was supported by grants from the National Natural Science Foundation of China (31991181, 31801859 and 32302581), the National Key Research and Development Program of China (2021YFF1000103), the Key Research and Development Program of Guangdong Province (2021B0707010005), the US National Science Foundation (IOS-1855585) and the Youth Innovation Program of the Chinese Academy of Agricultural Sciences (Y2023QC05).

Author contributions S.H. and J.Z. conceived and designed the research. J.Z., H.L., J.C. and X.C. performed most of the experiments and analyses. J.Z., H.L., J.C., X.C., J.R., J.W., Y.L. and Y.W. collected the phenotypic data. N.W., Z.Z., T.L., Yao Zhou, Yongfeng Zhou and G.Z. contributed to the bioinformatics analyses. L.M. contributed to the in vitro phosphorylation assays. R.D. and K.Z. contributed to the sensory evaluation assays. S.H., H.K., Z.F., T.L., Yao Zhou, Yongfeng Zhou and J.Z. coordinated the project. J.Z., H.L. and J.C. wrote the original draft article. S.H., H.K. and Z.F. revised the manuscript. S.H. and H.K. supervised the research. All authors read and approved the final manuscript.

Competing interests A patent on the use of Sl*CDPK27* and Sl*CDPK26* to improve fruit sugar content has been filed by S.H., J.Z., H.L., J.C. and G.Z. (CN202211616622.8; PCT/CN2023/138699). The other authors declare no competing interests.

Additional information

Supplementary information The online version contains supplementary material available at https://doi.org/10.1038/s41586-024-08186-2.

Correspondence and requests for materials should be addressed to Sanwen Huang.

Peer review information *Nature* thanks the anonymous reviewers for their contribution to the peer review of this work.

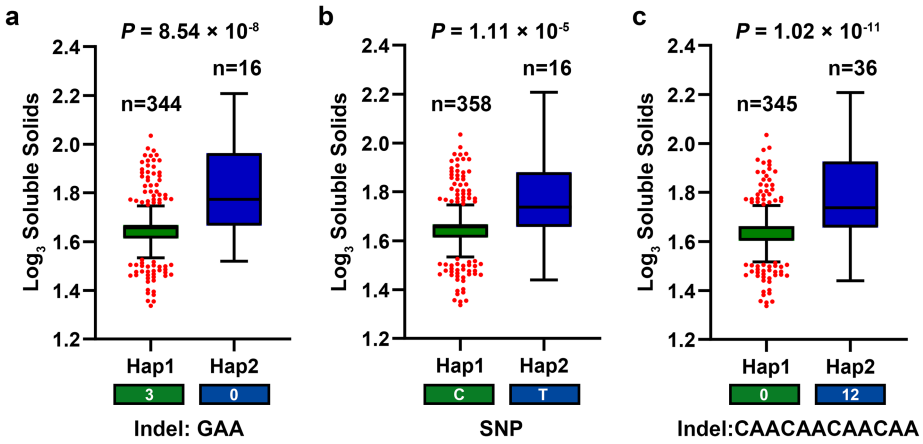

Extended Data Fig. 1 | Roles of the three key variations in total soluble solids content. a-c, Haplotype analysis of the 3-bp deletion (a), SNP (b) and 12-bp insertion (c), based on the total soluble solids content. Box plots represent the interquartile range, the line in the middle of each box represents the median, the whiskers represent the interquartile range, and the dots represent outlier points. Significant difference was determined by the two-tailed Student's *t* test.

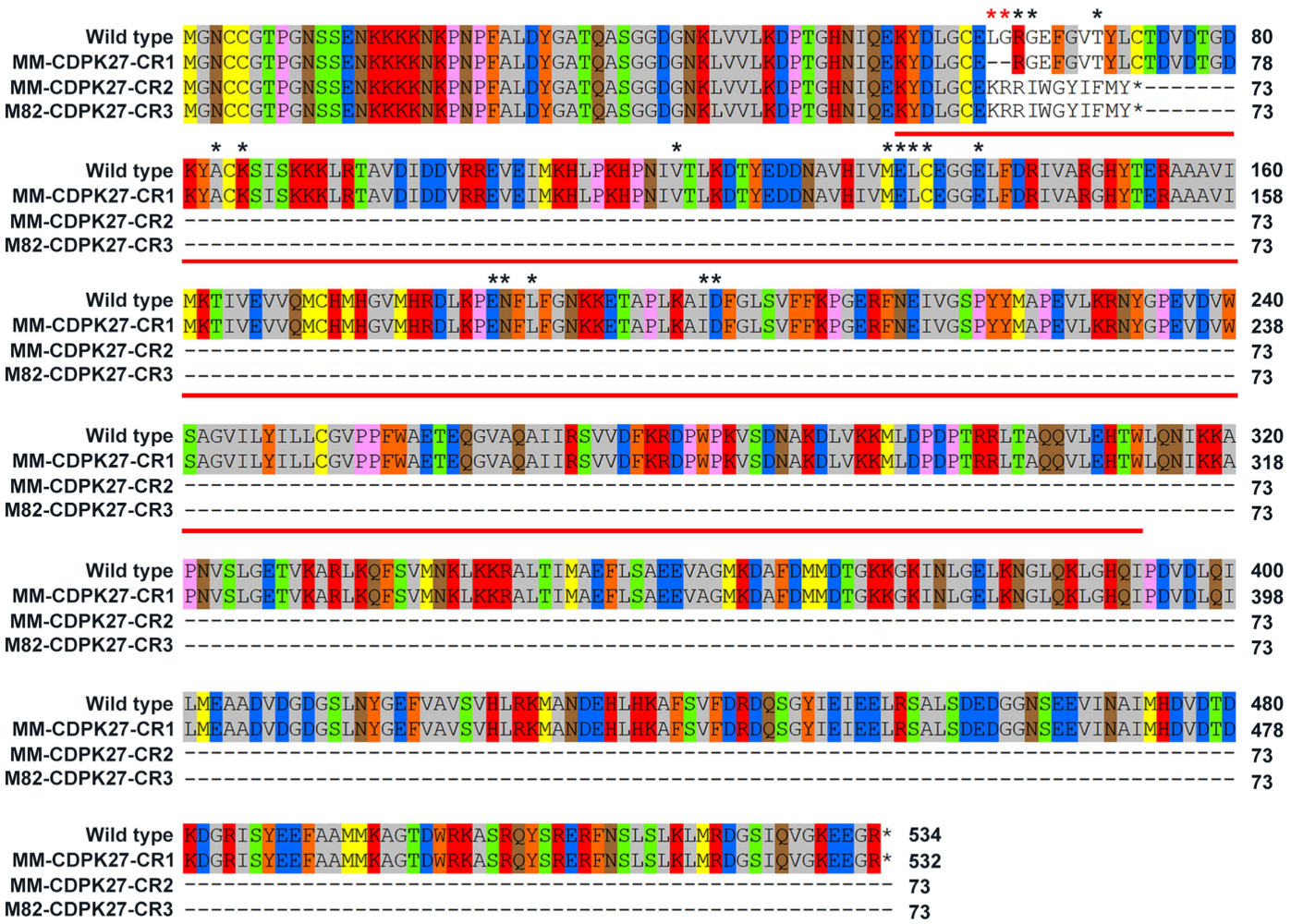

Extended Data Fig. 2 | Amino acid alignment of *Sl*CDPK27 in MM-CDPK27-CR1, MM-CDPK27-CR2 and M82-CDPK27-CR3 compared to the wild-type tomato line. The MM-CDPK27-CR1 lost two key amino acids in the kinase domain. The protein translation of MM-CDPK27-CR2 and M82-CDPK27-CR3 was premature. The kinase domain is underlined in red. Asterisks above the alignment represent 18 conserved residues that compose the feature of the ATP binding site in the kinase domain.

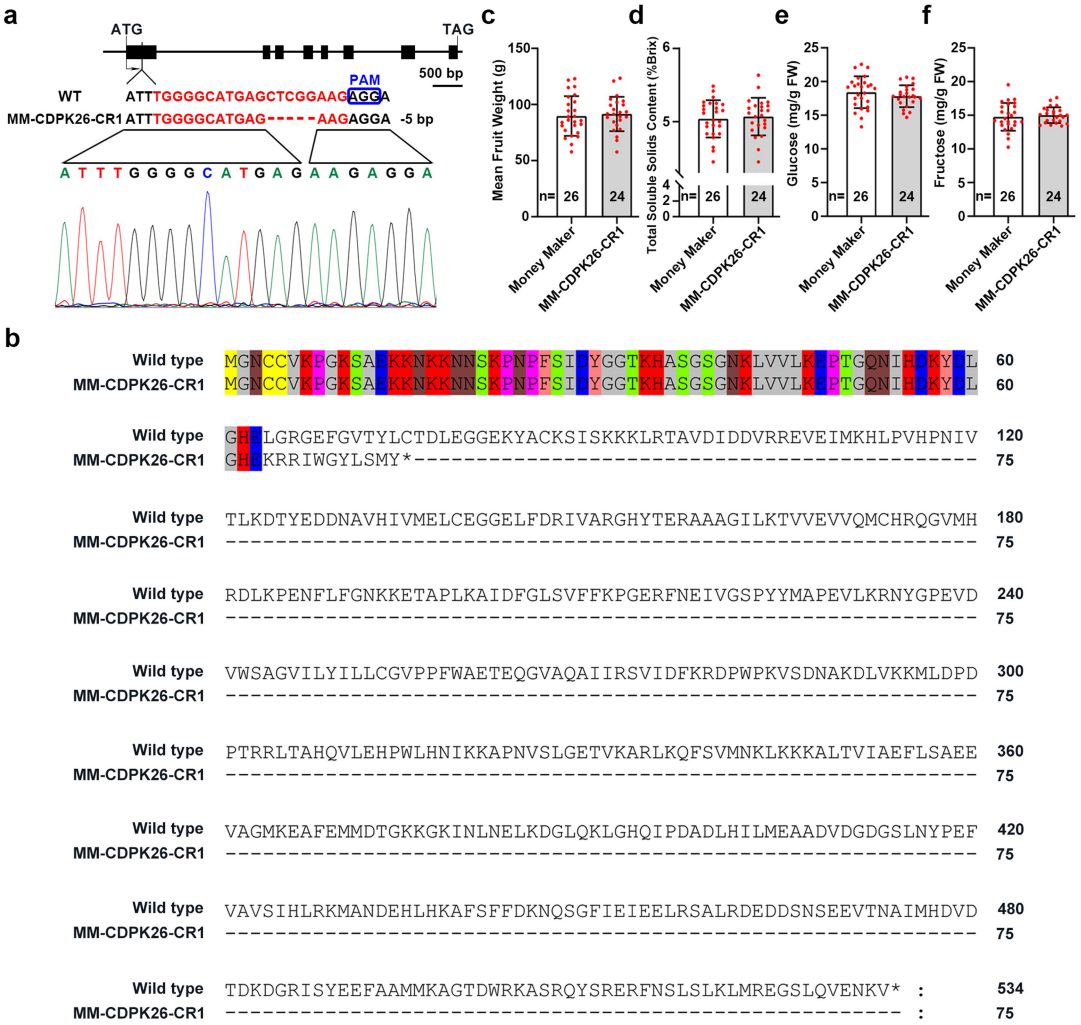

Extended Data Fig. 3 | Single deficiency in Sl*CDPK26* had little effects on sugar content. a, Generation of Sl*CDPK26* mutant. Sequences of Sl*CDPK26* in wild type and MM-CDPK26-CR1 mutants are shown. The sgRNA-targeted sequences are indicated in red, and the protospacer adjacent motif (PAM) sequence is highlighted in a blue rectangle. The deletion is indicated by a dashed line. **b**, Amino acid alignment of *Sl*CDPK26 in MM-CDPK26-CR1 compared to the wild-type tomato line. The protein translation of MM-CDPK26-CR1 was premature. **c-f**, MM-CDPK26-CR1 exhibited comparable fruit weight (c), total soluble solids (d), glucose (e) and fructose (f) contents, compared to wild-type plants. Values are means ± SD, n represents numbers of biologically independent samples. In c-f, a two-tailed Student's *t*-test was used to determine *P* values (see Source Data).

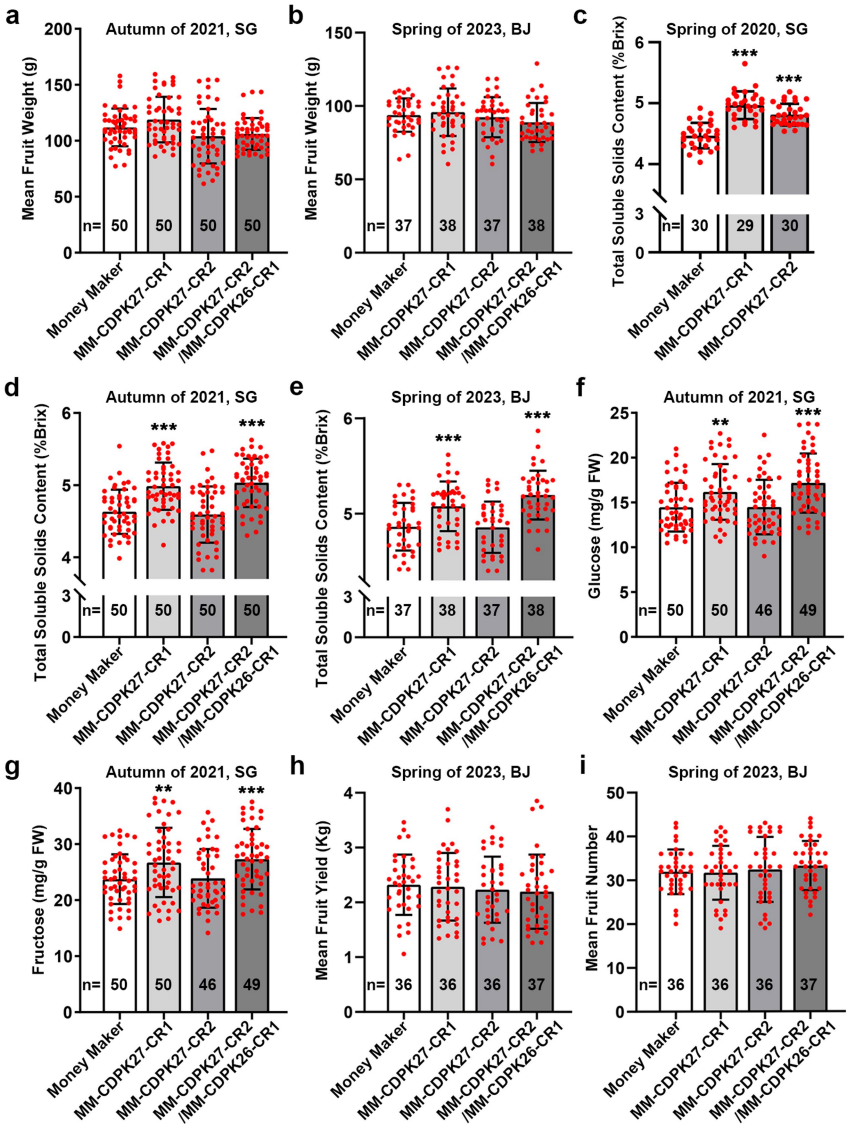

Extended Data Fig. 4 | Deficiency in Sl*CDPK26* enhances the effects of Sl*CDPK27* on sugar content. a-b, Fruit weight of sl*cdpk* mutant plants was not significantly different from that of wild-type plants. **c-g**, Comparison of total soluble solids (c to e), glucose (f), and fructose contents (g) between wild-type and sl*cdpk* mutant plants. **h-i**, The sl*cdpk* mutant plants exhibited comparable fruit yield (h), and fruit number (i) with wild-type plants. SG, Shouguang (Shandong, China); BJ, Beijing. Values are means ± SD, n represents numbers of biologically independent samples. In a-i, a two-tailed Student's *t*-test was used to determine *P* values (see Source Data). $^{**}P < 0.01$, $^{***}P < 0.001$, compared to the wild-type (Money Maker) plants.

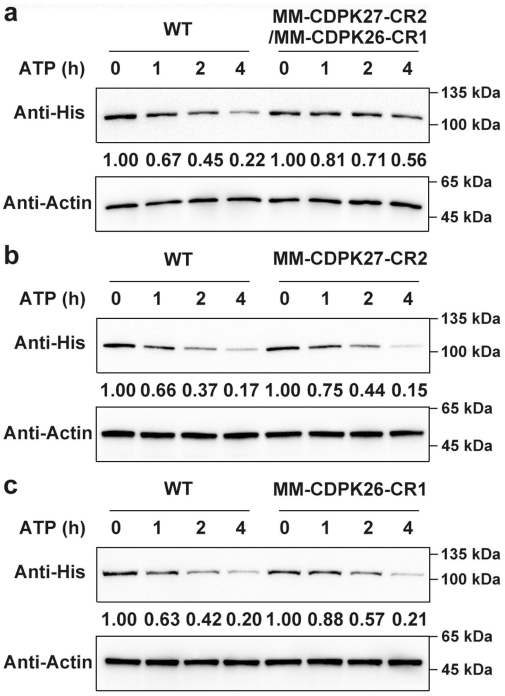

Extended Data Fig. 5 | Cell-free degradation assays. a, Compared with wild type, *Sl*SUS3 showed obvious slower degradation rate in the extracts of MM-CDPK27-CR2/MM-CDPK26-CR1 double mutant. **b-c**, *Sl*SUS3 showed slight slower degradation rate in the extracts of MM-CDPK27-CR2 (b) or MM-CDPK26-CR1 (c) single mutants, compared to the wild-type extracts. All of these cell-free degradation assays were repeated three times with similar results.

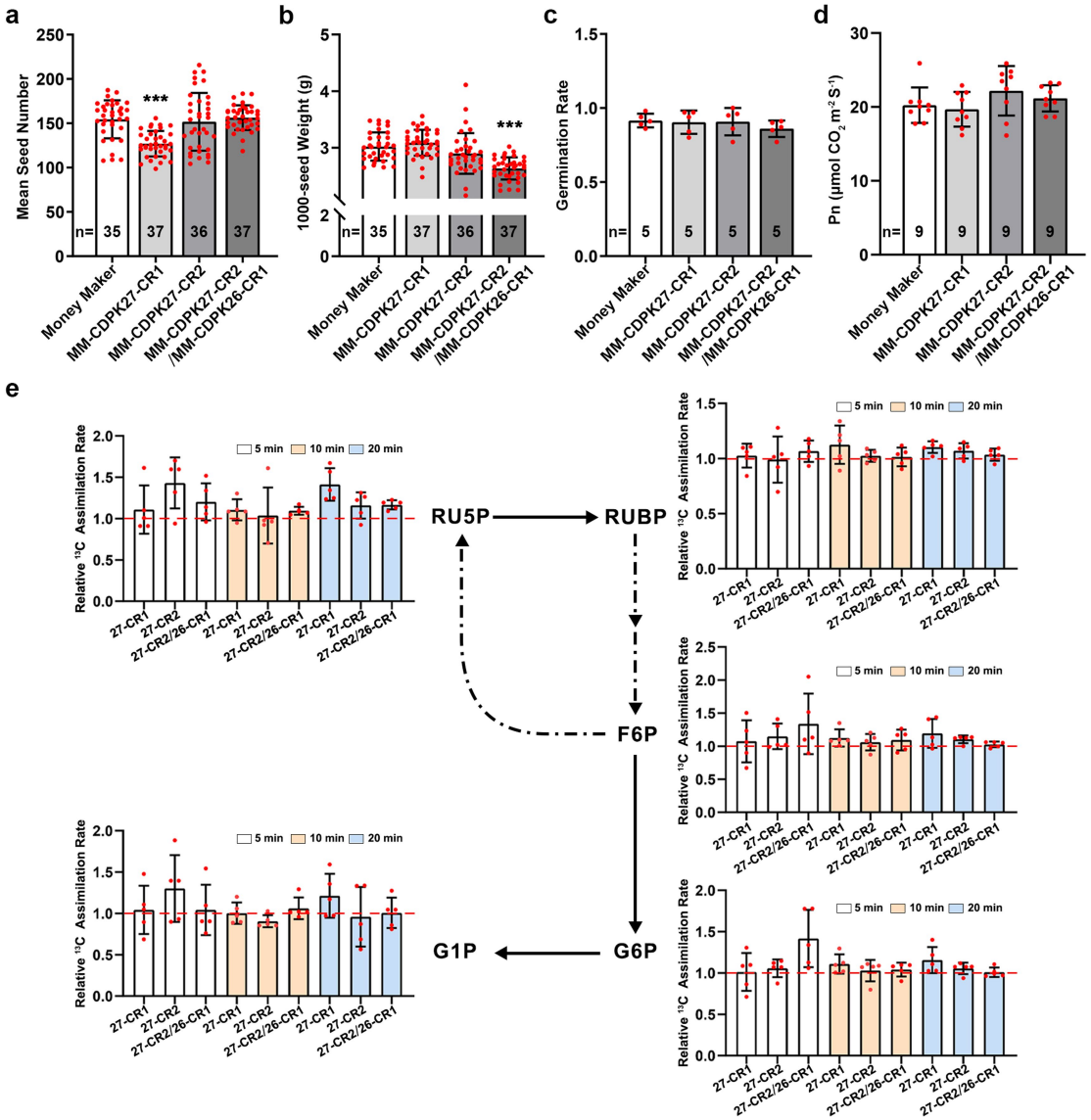

Extended Data Fig. 6 | Sl*CDPK* mutants contain fewer, lighter seeds, without influencing photosynthesis. a-c, Comparison of seed number (a), 1000-seed weight (b), and seed germination rate (c) between wild-type, MM-CDPK27-CR1, MM-CDPK27-CR2 and MM-CDPK27-CR2/MM-CDPK26-CR1 double mutant plants. **d**, Net photosynthesis rate (Pn) measured with the LICOR-6800 XT instrument. In a-d, values are means ± SD, n represents numbers of biologically independent samples. Two-tailed Student's *t*-test was used to determine *P* values (see Source Data). ***$P < 0.001$, compared to the wild-type (Money Maker) plants. **e**, Relative carbon assimilation rate of the sl*cdpk* mutants, as calculated relative to wild-type (Money Maker) plants during a 20 min $^{13}CO_2$ labeling process. Values are means ± SD (n = 5 independent replicates). RUBP, ribulose-1,5-bisphosphate; RU5P, ribulose-5-phosphate; F6P, fructose-6-phosphate; G6P, glucose-6-phosphate; G1P, glucose-1-phosphate; 27-CR1, MM-CDPK27-CR1; 27-CR2, MM-CDPK27-CR2; 26-CR1, MM-CDPK26-CR1.

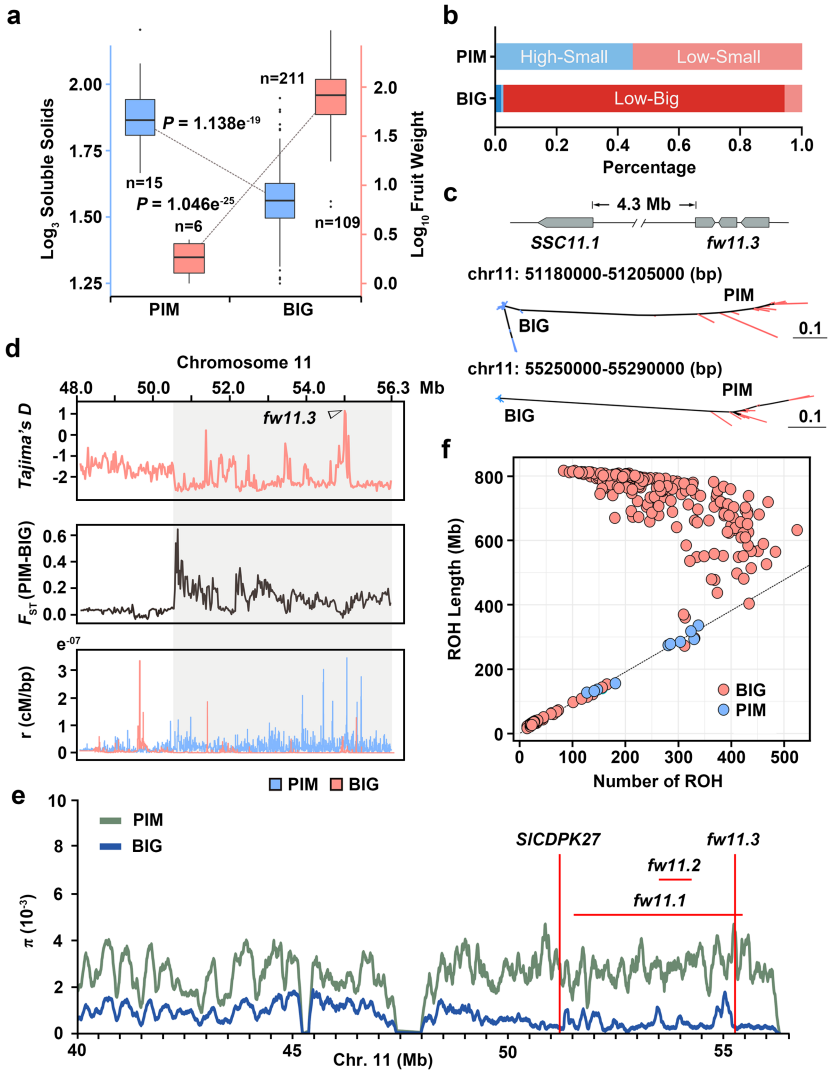

Extended Data Fig. 7 | Co-evolution of the *SSC11.1* and *fw* loci. a, Differences in soluble solids content and fruit weight between the wild (PIM) and cultivated (BIG) populations. Box plots represent the interquartile range; the line in the middle of each box represents the median, the whiskers represent the interquartile range, and the dots represent outlier points. Significant difference was determined by the two-tailed Student's *t* test. Number of accessions in each group is indicated by n. **b**, Haplotype frequencies of *SSC11.1* and *fw11.3* among PIM and BIG populations. High represented the high-SSC allele, Low represented the low-SSC allele. Big indicates the allele associated with big fruit, Small indicates the allele associated with small fruit. The striking haplotypes (frequency > 30%) are highlighted. **c**, Phylogenetic analysis of the *SSC11.1* (ch11_51.180–51.205 Mb; SL2.50) and *fw11.3* (ch11_55.250–55.290 Mb; SL2.50) loci. *SSC11.1* is about 4.3 Mb from *fw11.3*. **d**, Genetic statistics of *Tajima's D*, differentiation (F_{ST}) and per-generation, per-base recombination rate (r) in the ch11_48.0–56.3 Mb (SL2.50). **e**, Distribution of nucleotide diversity (π) of the PIM (green) and BIG (blue) lines. *SlCDPK27* is located within the large selective sweep region harboring three fruit mass QTLs on the end of chromosome 11. **f**, Genome-wide ROHs analysis of accessions among the PIM and BIG populations. The x-axis indicates the number of ROHs, y-axis indicates the total length of genomic ROHs. The dotted line was estimated based on the PIM population.

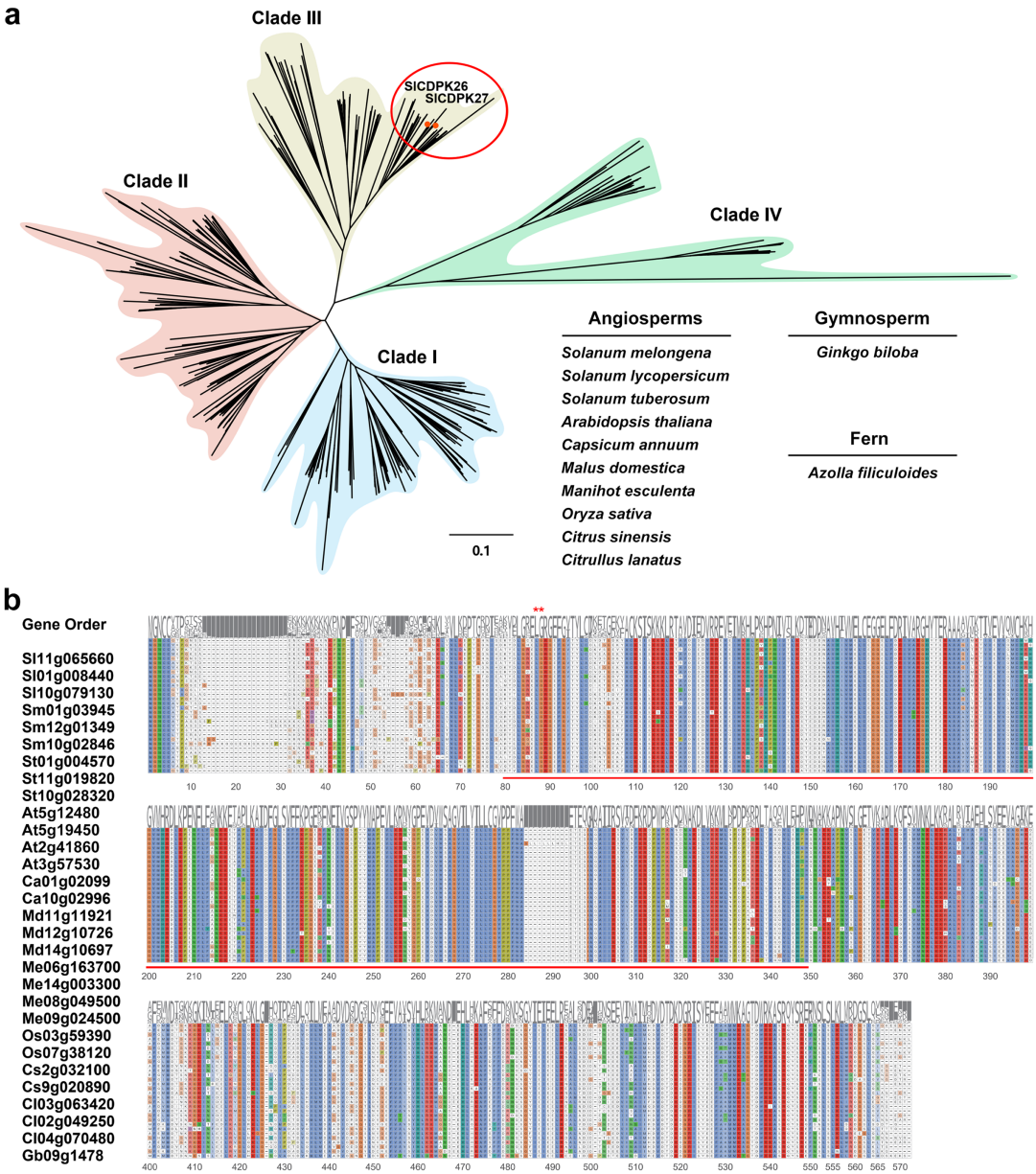

Extended Data Fig. 8 | Phylogenetic analysis of *Sl*CDPK27 and *Sl*CDPK26. **a**, Phylogenetic tree of CDPK orthologs across 12 plant genomes, including a fern (*Azolla filiculoides*), a gymnosperm (*Ginkgo biloba*) and 10 angiosperm crops (*Solanum lycopersicum*, *Solanum melongena*, *Solanum tuberosum*, *Arabidopsis thaliana*, *Capsicum annuum*, *Malus domestica*, *Manihot esculenta*, *Oryza sativa*, *Citrus sinensis* and *Citrullus lanatus*). The orthologs used for further sequence alignment in b are marked in red circles. **b**, Amino acid alignment of *Sl*CDPK27, *Sl*CDPK26 and their orthologs. The kinase domain is underlined in red. The red asterisks above the alignment represent the two amino acids deleted in MM-CDPK27-CR1.

nature portfolio

Corresponding author(s): Sanwen Huang

Last updated by author(s): Sep 1, 2024

Reporting Summary

Nature Portfolio wishes to improve the reproducibility of the work that we publish. This form provides structure for consistency and transparency in reporting. For further information on Nature Portfolio policies, see our Editorial Policies and the Editorial Policy Checklist.

Statistics

For all statistical analyses, confirm that the following items are present in the figure legend, table legend, main text, or Methods section.

n/a	Confirmed
☐	☒ The exact sample size (*n*) for each experimental group/condition, given as a discrete number and unit of measurement
☐	☒ A statement on whether measurements were taken from distinct samples or whether the same sample was measured repeatedly
☐	☒ The statistical test(s) used AND whether they are one- or two-sided *Only common tests should be described solely by name; describe more complex techniques in the Methods section.*
☒	☐ A description of all covariates tested
☐	☒ A description of any assumptions or corrections, such as tests of normality and adjustment for multiple comparisons
☐	☒ A full description of the statistical parameters including central tendency (e.g. means) or other basic estimates (e.g. regression coefficient) AND variation (e.g. standard deviation) or associated estimates of uncertainty (e.g. confidence intervals)
☐	☒ For null hypothesis testing, the test statistic (e.g. *F*, *t*, *r*) with confidence intervals, effect sizes, degrees of freedom and *P* value noted *Give P values as exact values whenever suitable.*
☒	☐ For Bayesian analysis, information on the choice of priors and Markov chain Monte Carlo settings
☒	☐ For hierarchical and complex designs, identification of the appropriate level for tests and full reporting of outcomes
☒	☐ Estimates of effect sizes (e.g. Cohen's *d*, Pearson's *r*), indicating how they were calculated

Our web collection on statistics for biologists contains articles on many of the points above.

Software and code

Policy information about availability of computer code

Data collection	SSC were measured by a digital refractometer (PAL-1, ATAGO, JPN) Saccharide content was measured by UPLC-MS/MS (ACQUITY UPLC I-Class-Xevo TQ-S Micro, Waters) Bio-Rad CFX96 with CFX Maestro 1.1 software was used to qPCR analysis The fluorescence signal was detected using a confocal microscopy (Leica SP8) The LUC activity was analyzed using the Night SHADE LB985 (Berthold) and Tanon-5200 image system The Net photosynthesis rate was measured with the LICOR-6800 XT instrument
Data analysis	Image analysis: ImageJ (version 1.45) Statistical analysis: GraphPad Prism (version 8.00) Phylogenetic analysis: MEGA (version 11.0.10), hmmer (version 3.4), MAFFT (version 7.525), ggmsa (version 3.19) Saccharide content analysis: MassLynx V4.1 (Waters) Genetic statistics analysis: IQTREE (version 2.1.4), VCFtools (version 0.1.16), PLINK (version 1.90b6.21), ggplot2 (version 3.4.4)

For manuscripts utilizing custom algorithms or software that are central to the research but not yet described in published literature, software must be made available to editors and reviewers. We strongly encourage code deposition in a community repository (e.g. GitHub). See the Nature Portfolio guidelines for submitting code & software for further information.

Data

Policy information about availability of data

All manuscripts must include a data availability statement. This statement should provide the following information, where applicable:

- Accession codes, unique identifiers, or web links for publicly available datasets
- A description of any restrictions on data availability
- For clinical datasets or third party data, please ensure that the statement adheres to our policy

All data are available within this Article and its Supplementary Information (Supplementary Tables 1-10). Original uncropped gel and blot images are provided in Supplementary Figs. 1-2. Original data points in graphs are shown in the Source Data files. HMM models were downloaded from the InterPro database (https://www.ebi.ac.uk/interpro/entry/pfam). Source data are provided with this paper.

Research involving human participants, their data, or biological material

Policy information about studies with human participants or human data. See also policy information about sex, gender (identity/presentation), and sexual orientation and race, ethnicity and racism.

Reporting on sex and gender	The sex and gender information of the participants for each of the sensory evaluation panel has not been collected.
Reporting on race, ethnicity, or other socially relevant groupings	NA
Population characteristics	In the sensory evaluation study, approx. 100 participants (age 20- to 59-years-old) were selected for each of the sensory test. These participants were required to be healthy and without any known oral diseases.
Recruitment	All participants were previously informed as to the sources of the genome-edited tomato materials and the sensory procedure and requirement, and signed informed consent forms before the sensory tests. The participants for each of the sensory test were recruited randomly, without any self-selection bias, except that the participants with any known oral diseases were excluded, because they may be insensitive to the sweetness. Participants are not limited by sex or gender, both males and females could participate in the sensory tests.
Ethics oversight	The sensory test followed the Declaration of Helsinki, and the experimental protocol was approved by the Ethical Committee of Agricultural Genomics Institute at Shenzhen, Chinese Academy of Agricultural Sciences.

Note that full information on the approval of the study protocol must also be provided in the manuscript.

Field-specific reporting

Please select the one below that is the best fit for your research. If you are not sure, read the appropriate sections before making your selection.

☒ Life sciences ☐ Behavioural & social sciences ☐ Ecological, evolutionary & environmental sciences

For a reference copy of the document with all sections, see nature.com/documents/nr-reporting-summary-flat.pdf

Life sciences study design

All studies must disclose on these points even when the disclosure is negative.

Sample size	No statistical methods were used to determine sample size. The sample size is described in the relevant figure legends and supplementary information. The 402 accessions were selected to calculate the allele frequency based on our previous study (Tieman et al., Science 2017, 355, 391-394). For agronomic traits in the field, sample sizes were chosen based on previous publications (Song et al., Nature 2023, 617: 118-124; Liu et al., Nature 2021, 590: 600-605; Tian et al., Science 2019, 365: 658-664).
Data exclusions	The plants, which were diseased or grown in the guard rows, were marked and were excluded from the analyses.
Replication	Three biological replicates with three technical replicates were used in the qRT-PCR experiment. For the subcellular localization, histological analysis, Y2H, LCI and cell-free protein degradation assays, the results are representative of three independent experiments. Three independent transgenic knock-out lines were generated for SlCDPK27. All of these experiments were successfully repeated.
Randomization	All samples were arranged randomly into experimental groups.
Blinding	For molecular biology experiments, bias could not be introduced since samples were treated identically and collected randomly. The investigation of agronomic traits was performed without prior knowledge of the results, blind was also not applied. For the sensory evaluation of sweetness assay, each sample was labeled with random codes, and the paired samples were presented to the sensory assessors, for sensory evaluation, in a balanced order.

Reporting for specific materials, systems and methods

We require information from authors about some types of materials, experimental systems and methods used in many studies. Here, indicate whether each material, system or method listed is relevant to your study. If you are not sure if a list item applies to your research, read the appropriate section before selecting a response.

Materials & experimental systems

n/a	Involved in the study
☐	☒ Antibodies
☒	☐ Eukaryotic cell lines
☒	☐ Palaeontology and archaeology
☒	☐ Animals and other organisms
☒	☐ Clinical data
☒	☐ Dual use research of concern
☐	☒ Plants

Methods

n/a	Involved in the study
☒	☐ ChIP-seq
☒	☐ Flow cytometry
☒	☐ MRI-based neuroimaging

Antibodies

Antibodies used

Anti-His (MBL, Cat# D291-3, 1:3,000 dilution)
Anti-Actin (Sigma, Cat# A0480, 1:10,000 dilution)
Horseradish peroxidase-conjugated goat anti-mouse IgG (H+L) (ZSGB-BIO, Cat#ZB-2305, 1:10,000 dilution)
Horseradish Peroxidase-conjugated goat anti-rabbit IgG (H+L) (ZSGB-BIO, Cat#ZB-2301, 1:10,000 dilution)
Anti-SlCDPK27 (custom-developed by Shanghai Youke Biotechnology Co., Ltd, 1:100 dilution for IP-MS assay, 1:2,000 dilution for western blot assay)

Validation

Validation statements and experiments can be obtained from the following websites and publications:
Anti-His (https://www.mblbio.com/bio/g/dtl/A/?pcd=D291-3)
Anti-Actin (https://www.sigmaaldrich.com/CG/en/product/sigma/a0480)
Horseradish peroxidase-conjugated goat anti-mouse IgG (H+L) (http://www.zsbio.com/product/ZB-2305)
Horseradish Peroxidase-conjugated goat anti-rabbit IgG (H+L) (http://www.zsbio.com/product/ZB-2301)
Residues 6-20 of SlCDPK27 was used to make antibodies by Shanghai Youke Biotechnology Co., Ltd, and S. lycopersicum Money Maker (MM) and SlCDPK27-CR2 were used to validate anti-SlCDPK27 antibody.

Plants

Seed stocks

The detailed information of all the 402 accessions used in this study are listed in Supplementary Table 8.

Novel plant genotypes

The SlCDPK27 and SlCDPK26 mutants with 6-bp or 5-bp deletions were generated by CRISPR/Cas9 system in S. lycopersicum Money Maker (MM) or the processing variety M82.

Authentication

The SlCDPK27 and SlCDPK26 mutants were verified by PCR and sequencing. All experiments were performed using homozygous lines without T-DNA integration. And all of the potential off-target sites for both SlCDPK27 and SlCDPK26, were tested by PCR and sequencing.